https://doi.org/10.1016/j.engstruct.2021.112301

Damage-control steel frames equipped with SMA connections and ductile links subjected to near-field earthquake motions: A spectral energy factor model

Xuhong Zhou[a, b], Huanyang Zhang[a], Ke Ke[b, a *], Lihua Guo[b], Michael CH Yam[c, d]

[a] *Hunan Provincial Key Laboratory on Damage Diagnosis for Engineering Structures, Hunan University, Changsha, China*

[b] *Key Laboratory of New Technology for Construction of Cities in Mountain Area, School of Civil Engineering, Chongqing University, Chongqing, China*

[c] *Department of Building and Real Estate, The Hong Kong Polytechnic University, Hong Kong, China*

[d] *Chinese National Engineering Research Centre for Steel Construction (Hong Kong Branch), The Hong Kong Polytechnic University, Hong Kong, China*

Abstract: To achieve a delicate balance between self-centring behaviour and energy dissipation, it was proposed to develop the damage-control steel frame equipped with shape memory alloy (SMA) connections and ductile links showing the partially self-centring behaviour. This paper examined the inelastic seismic demand of the novel structure, and the emphasis was given to the spectral energy factor of the system subjected to near-field earthquake motions. Based on single-degree-of-freedom (SDF) systems representing the novel structure and a near-field earthquake database, nonlinear spectral analyses were performed considering a wide range of structural period and hysteretic parameters, and more than 25 million energy factors were obtained. The probabilistic characteristics of the energy factors were examined in detail. The analysis database confirmed that the energy factors were sensitive to structural period and hysteretic parameters. In addition, a right-skewed distribution feature of the energy factors was observed. Thus, a spectral energy factor model for damage-control steel frames equipped with SMA connections and ductile links was developed using the lognormal distribution model. Nonlinear regression analyses were conducted to develop a series of prediction equations. The good agreement between the histograms of the energy factor and predictions by the regression equations confirmed the adequacy of the proposed model. The proposed model was eventually applied to evaluating the damage-control behaviour of a prototype structure under near-field earthquake motions, and the sufficiency of the model for assessing the structural damage-control behaviour from a statistic perspective was confirmed.

Keywords: Shape memory alloy; damage-control; partially self-centring; energy factor; hysteretic model

---

Corresponding author keke@hnu.edu.cn, kerk.ke@outlook.com

1. Introduction

Steel moment resisting frames (MRFs) are widely used in building structures and have long been reckoned as effective seismic resistant systems. In particular, the conventional ductility-based seismic design methodology for steel MRFs generally aims to produce plastic hinges at the beam ends and column bases to dissipate seismic energy and achieve ductile behaviour. Consequently, excessive exploitation of the inelastic energy dissipation capacity of structural members and connections in a steel MRF might lead to significant structural damages and post-earthquake residual deformations, as demonstrated by recent earthquake events and seismic loss estimations [1, 2]. Recent research findings [2] indicated that a steel MRF designed to follow the ductility-based design philosophy may have a high possibility of suffering a total economic loss even in the event of a design-level earthquake. This is because the post-earthquake residual deformation generally leads to a long period of occupancy suspension to enable repair work or may even result in complete demolition of the structure. The lessons from recent earthquake attacks signal the demand of more sustainable steel frames with a higher level of seismic resistance, and novel structures with improved cyclic behaviour and controllable post-earthquake performance is actively pursued by the research community.

Hopefully, recent explorations of the "self-centring" technology produced steel frames with reduced post-earthquake residual deformations. In parallel with the structural-based self-centring technology that enables recentring behaviour with post-tensioned devices [3-5], research works also indicate that the self-centring performance may be realised using Shape Memory Alloys (SMAs) [6-11]. Because the superelasticity of SMAs enables the material to

restore the deformed shapes upon unloading, novel self-centring beam-to-column connections equipped with SMAs have emerged as compelling candidates for steel frame structures. For example, Ocel et al. [12] modified the conventional welded flange-bolted web connection and replaced the welded connection in the flange area by SMA bars. Yam and co-workers [13, 14] explored the seismic performance of stiffened extended end-plate (SEE) connections equipped with SMA bolts considering varied connection configurations. Wang et al. [15] studied the behaviour of a novel column base equipped with SMA bars. To examine the influence of SMA connections on the behaviour of structural systems, DesRoches et al. [16] studied seismic responses of steel frames equipped with SMA connections numerically, and the results showed that the structural seismic demand is affected by the SMA connections. Based on nonlinear dynamic analysis of an ensemble of prototype systems, Sultana and Youssef [17] further confirmed that the implementation of SMA connections in a steel MRFs could profoundly influence the structural seismic response and contributes to mitigated post-earthquake residual deformations. However, the research works mentioned above generally focused on the hysteretic behaviour of SMA connections and general seismic responses of structural systems equipped with SMAs, whereas optimised arrangement strategy of SMA connections in steel frames was not clearly examined, and quantitative methods for prescribing the inelastic seismic demand from a structural perspective were not emphasised.

In particular, although nonlinear response history analysis (NL-RHA) procedure based on the numerical model of a structure may be used to quantify the inelastic seismic demand of steel frames equipped with SMA connections rigorously, practitioners generally prefer to

use static procedures (e.g. direct design method or nonlinear static procedure) to conduct a preliminary design of a new structure or assessment of an existing system prior to performing NL-RHA. In this context, the essence of a successful design or evaluation is the reasonable prescription of the inelastic spectral demand indices of the structure subjected to earthquake motions. To shed insightful lights on the inelastic seismic demands of systems showing the self-centring behaviour, research works were carried out in recent decades. For example, Christopoulos et al. [18] quantified the ductility, acceleration and cumulative energy demand of self-centring structures based on spectral analyses of single-degree-of-freedom (SDF) oscillator with the bilinear flag-shaped hysteretic model. Zhang et al. [19] studied the inelastic displacement demand of bilinear flag-shaped self-centring SDOF systems on the stiff soil. Recognising the attractiveness of using the energy balance concept in seismic design, research interests have been directed to energy-based spectral model for quantifying the inelastic seismic demands of self-centring systems. For instance, based on the modified Housner equation [20-22], Ke et al. [23] developed the energy factor demand spectra of bilinear flag-shaped oscillators, which united the strength and deformation demand. Later, Qiu and Zhu. [24] developed a performance-based plastic design methodology for self-centring braced steel frame structures using the energy factor as the core demand index. Zhou et al. [25, 26] examined the input energy and hysteretic energy demand spectra of bilinear self-centring SDF systems. Nonetheless, the research mentioned above may only apply to self-centring steel frames exhibiting perfectly self-centring behaviour (i.e. flag-shaped hysteretic responses). In addition, the statistic demand index (e.g. the mean value) was generally emphasised in

106 the previous studies for practical simplicity, whereas probabilistic characteristics of the
107 demand indices were not clearly examined. In this context, more research efforts are
108 needed to bridge the knowledge gap towards rational quantifications of novel steel frames
109 equipped with SMA connections which exhibit varied hysteretic behaviour, and a practical
110 seismic demand model which can be used to characterise inelastic seismic demands of
111 novel self-centring steel frames equipped with SMA connections is also required.

112 In light of the above, the primary objective of the present study was to quantify the
113 inelastic seismic demand of a novel steel frame equipped with SMAs, i.e. damage-control
114 steel frames equipped with SMA connections and ductile energy dissipation links showing
115 the partially self-centring behaviour, and the focus was given to a spectral energy factor
116 model which may be used to prescribe the strength demand and the deformation demand
117 concurrently. Specifically, it was proposed that superelastic SMA connections and ductile
118 links arranged in the "hybrid energy dissipation bays" to be the primary source of inelastic
119 energy dissipation under an earthquake motion. A wise combination of superelastic SMA
120 connections and ductile links may contribute to a delicate balance between the recentring
121 ability and the energy dissipation capacity, and the damage-control behaviour of a steel
122 frame may be ensured as inelasticity was restricted in the SMA connections and ductile
123 links for a reasonable deformation spectrum. Based on the hysteretic model of the system
124 and a database of near-field earthquake motions, the inelastic demand of a steel frame
125 equipped with SMA connections and ductile links was quantified by developing the energy
126 factor spectra of equivalent single-degree-of-freedom (SDF) systems representing the novel
127 structure. The influence of the hysteretic parameters on the energy factor spectra was

carefully examined, and the probabilistic features of the demand spectra were characterised. Based on the analysis database composed of more than 25 million data points, a spectral energy factor model for quantifying the seismic demand of steel frames equipped with SMA connections and ductile links showing the partially self-centring behaviour was developed for engineering applications. To confirm the adequacy of the proposed model, a prototype structure was developed, and the accuracy of the numerical modelling techniques was justified by the available laboratory test data. The proposed energy factor model was applied to evaluating the damage-control behaviour of the prototype structure under an ensemble of near-field earthquake motions. The hysteretic model, damage-control behaviour of the prototype system in a reasonable deformation range and the effectiveness of the system for mitigating the post-earthquake residual deformations was confirmed by cyclic pushover analysis and NL-RHAs.

2. Notion and hysteretic behaviour of partially self-centring steel frames equipped with SMA connections and ductile links

2.1. Design concept

The notion of a damage-control steel frame equipped with SMA connections and ductile links is schematically shown in Fig. 1a. To achieve a reasonable balance between the recentring ability and the energy dissipation capacity, it is proposed that a "hybrid energy dissipation bay" is composed of superelastic SMA connections and ductile energy dissipation links. The excellent self-centring performance of the SMA connections can reduce the seismic loss caused by the post-earthquake residual deformation [27, 28]. As

shown in Fig. 1a, the SMA connection developed by Yam and colleagues [14] is equipped with external SMA bolts in steel washers, which contribute to moment resistance and self-centring restoring force. Note that the steel washer is playing a significant role in applying pre-tension on the SMA bolts, which contributes to enhanced self-centring behaviour and connectional stiffness [14]. In addition, high strength (HS) bolts equipped with SMA Belleville washers are incorporated in the internal bolt row, providing shear resistance. Note that the SMA Belleville washers also allow the HS bolts to release the tension force when the endplate rotates, and the permanent elongation of HS bolts may be minimised. The effectiveness of adding HS bolt with SMA Belleville washers in the connection for enhancing the behaviour of the connection has been verified by Fang et al. [14]. The deformed pattern of the novel SMA connection subjected to hogging action and the test evidence provided by Yam and co-workers [14] are reproduced in Fig. 1b. In general, it is expected that the hybrid energy dissipation bays offer inelastic energy dissipation for a wide deformation range under earthquake motions. In the meantime, the SMA connections and the main frame members (Fig. 1a) provide the recovery force in the damage-control stage, which contributes to pulling the structure close to the upright position and mitigates the post-earthquake deformations.

2.2. Hysteretic model and representative oscillator

The hysteretic behaviour of the novel damage-control steel frame may be quantified by a combination of the classical bilinear kinematic model [29] and bilinear flag-shaped model [18]. From the perspective of inelastic energy dissipation, it is proposed to trigger

the inelasticity inception of the SMA connections and ductile links simultaneously in the current study. Thus, a single-degree-of-freedom (SDF) oscillator governed by the bilinear partially self-centring hysteretic model with significant post-yielding stiffness ratio may be used to feature the hysteretic behaviour of a low-to-medium rise steel frame equipped with SMA connections and ductile links in the hybrid energy dissipation bays deforming in the damage-control stage. The hysteretic law is illustrated in Fig. 2. In particular, the bilinear force-displacement response can be used to characterise the skeleton response of the system, given by:

$$F = \begin{cases} K\delta & 0 \le \delta \le \delta_{\mathrm{y}} \\ \alpha K\delta + (1-\alpha)K\delta_{\mathrm{y}} & \delta > \delta_{\mathrm{y}} \end{cases} \quad (1)$$

where K= initial stiffness of the representative SDF oscillator; F = force quantity of the representative oscillator; δ = displacement quantity of the representative oscillator; δ_{y} = yield displacement of the representative oscillator characterising inelasticity inception of the SMA connection and ductile links and α = post-yielding stiffness ratio of the oscillator owing to the elastic main frame. In the hysteretic model, the parameter β defined as the energy ratio (Fig. 2) controls the unloading path. Note that in cases where $\beta \le 0.5$, it comes down to the conventional bilinear flag-shaped hysteretic law [18]. In the scenario with β = 1, the oscillator turns to be a bilinear kinematic system [29]. It is worth noting that the hysteretic model is applicable for a structure deforming in the damage-control stage where the main frame members remain generally elastic. The adequacy of the hysteretic model for characterising the cyclic responses of a damage-control steel frame equipped with SMA connections and ductile links will be justified in later sections. In practical

193 engineering, an iterative procedure can be adopted in the design phase to ensure the
194 expected yielding sequence of SMA connections and ductile links in the energy dissipation
195 bays, and the yield drift of the SMA connections can be estimated based on research
196 findings in [14].

197

198 **3. Construction of energy factor spectra**

199 *3.1. Governing equation and energy factor of the representative SDF system*

200 The normalised governing equation of the representative partially self-centring SDF
201 oscillator related to the corresponding elastic system is given by

202 $$\ddot{\mu}_s + 2\xi\omega\dot{\mu}_s + \omega^2\bar{F}(\mu_s,\alpha,\beta) = -\omega^2\frac{F_e}{F_y}\frac{\ddot{\delta}_g}{S_a} \quad (2)$$

203 where μ_s = normalised displacement quantity (δ / δ_y), which is defined as the ductility;
204 $\dot{\mu}_s$ = normalised velocity of the representative SDF oscillator ($\dot{\delta} / \delta_y$); $\ddot{\delta}$ = acceleration
205 of the earthquake motion; $\ddot{\mu}_s$ = normalised acceleration ($\ddot{\delta} / \delta_y$); $\bar{F}(\mu_s,\alpha,\beta)$ =
206 normalised restoring force of the representative SDF oscillator, which is governed by the
207 hysteretic model mentioned in Section 2; ξ = damping ratio; ω = frequency of the
208 associated elastic SDF oscillator; F_e = peak force of the associated elastic SDF oscillator
209 under the earthquake motion and S_a = pseudo acceleration coefficient.

210 The energy factor of the SDF oscillator representing a steel frame equipped with SMA
211 connections and ductile links is defined as the ratio of the covered area of the bilinear
212 skeleton pushover response to that of the associated elastic SDF system upon the expected
213 peak deformation (i.e. $\mu_s = \mu$, where μ is the expected ductility factor), as shown in Fig. 3.
214 The expression of the energy factor of a bilinear partially self-centring SDF oscillator is

given by

$$\gamma = 2\chi\mu - \chi + \alpha\chi(\mu - 1)^2 \tag{3}$$

$$\chi(T;\mu;\alpha;\beta;\xi) = [\frac{F_y(T;\mu;\alpha;\beta;\xi)}{F_e(T;\xi)}]^2 \tag{4}$$

where T = vibration period of the representative SDF oscillator and $F_y(T;\mu;\alpha;\beta;\xi)$ = yield force of the representative oscillator characterising inelasticity inception of the SMA connection and ductile links. Note that the energy factor of a SDF oscillator may be obtained using a constant-ductility-based method [30]. As the emphasis of the current study is given to the novel steel frames showing the partially self-centring behaviour, the boundary condition $0.5 < \beta < 1.0$ is considered.

3.2. Earthquake motions and parameter spectrum

In this work, an earthquake motion database was developed as input excitations. Recognising that near-field earthquake motions with pulse-like characteristics may import massive energy into a structure instantly, exposing a steel frame to much higher risks of failure, the research focus of the present study was given to near-field earthquake motions. To develop a ground motion database with generality, 320 realistic near-field earthquake motion records with evident velocity pulses recorded worldwide were selected from PEER database [31]. Note that these ground motions had a magnitude ranging from 5.5 to 7.9, and all the records were captured at stations close to the fault-rupture (with a distance below or equal to 30.5 km). The peak ground acceleration (PGA) of the earthquake motions ranged from 0.09 g to 1.74 g. Note that these ground motion records have been also used in the literature [32, 33] to feature the characteristics of near-field earthquake

motions and quantify inelastic seismic demands of structures. The acceleration spectra of these earthquake motions (damping ratio of 5%) plotted against logarithmic coordinates are shown in Fig. 4. More detailed information about the earthquake motions is included in the supplemental material package.

To offer in-depth insights into the influence of the hysteretic parameters on the energy factor of the SDF oscillator representing damage-control steel frames equipped with SMA connections and ductile links, inelastic spectral analyses of partially self-centring SDF systems with varied hysteretic parameters were performed. In the current study, nine levels of the post-yielding stiffness ratio (α) increased from 0 to 0.5 (i.e. α = 0, 0.01, 0.02, 0.03, 0.04, 0.05, 0.1, 0.3 and 0.5) were included in the parameter matrix. Note that this factor may characterise the relative stiffness of the main frame and the hybrid energy dissipation bays. The energy ratio (β) ranged from 0.6 to 0.9 was considered to examine the influence of combination strategies of SMA connections and ductile links. The ductility was varied from 1.25 to 10 with an increment of 0.25. It is worth noting that a damping ratio varied from 2% to 5% was reckoned appropriate for steel structures, and a relatively significant damping ratio may be used to feature the effect of non-structural elements and facades when the system was subjected to strong earthquake motions. Therefore, the damping ratio (ξ) of 5% was assumed in all the analyses, and the rationale was confirmed in the literature [34]. For comparison, the energy factors of perfectly self-centring systems (β = 0.1) were also included in the analysis database. In summary, 9×5×36×50×320 = 25,920,000 energy factors of the representative SDF oscillators were obtained.

4. Results database and discussions

4.1. Overview and influences of hysteretic parameters on the mean energy factor

Representative mean energy factor spectra of the SDF oscillators are plotted against the vibration period (T), and results with $T \leq 0.4$ s and $T > 0.4$ s are shown in Fig. 5a and Fig. 5b, respectively. The general trend of the energy factor of the partially self-centring SDF oscillators ($\beta > 0.5$) was similar to those of perfectly self-centring counterparts ($\beta = 0.1$). It can be seen that the mean energy factor generally decreases with an increasing period, and this trend was more evident in cases with a significant ductility factor. According to Fig. 5a, it is evident that an increasing post-yielding stiffness ratio generally leads to a decreasing energy factor (generally $\gamma > 1$) for the system in the short-period region ($T \leq 0.4$ s). For SDF systems in the longer period region, as shown in Fig. 5b, the reversed trend (generally $\gamma < 1$) can be characterised. For instance, according to the case of $\beta = 0.6$ and $\mu = 6$ in Fig. 5a, it is evident that an increasing post-yielding stiffness ratio from 0.05 to 0.5 leads to a decreasing mean energy factor for the system in the short-period region ($T \leq 0.4$ s). For SDF systems in the period region equal to or above 0.5 s as shown in Fig. 5b (i.e. the case of $\beta = 0.6$ and $\mu = 6$), the mean energy factor increases with the post-yielding stiffness ratio. Realising that the fundamental period of a steel frame generally falls within the period region with $T > 0.4$ s [35], special caution may need to be exercised when designing the post-yielding stiffness ratio of a steel frame equipped with SMA connections and ductile links due to the rising seismic demand. As for the influence of the target ductility factor (μ), it can be confirmed from Fig. 5a that an increasing target ductility factor may trigger drastic increase of the energy factor for short-period systems, whereas

281 the opposite trend was seen in cases with a longer period, as shown by Fig. 5b. The figure
282 also shows that the influence of the energy ratio (β) on the mean energy factor of
283 short-period systems with an insignificant ductility is not evident. Comparatively, an
284 increasing energy ratio results in a decrease of the mean energy factor of systems in the
285 longer period region, which is more pronounced for cases with significant ductility factors,
286 as can be seen from Fig. 5b. In general, it can be seen that the influence of the
287 post-yielding stiffness ratio and the ductility on the energy factor of partially self-centring
288 SDF systems is in line with the bilinear kinematic SDF systems [36]. The reasons for the
289 observed phenomena have also been discussed in [37]. The influence of the energy ratio on
290 the energy factor is also echoed by research works conducted by Christopoulos et al. [18].
291 Again, recalling that the fundamental vibration period of a multi-storey steel frame
292 generally falls in the relatively long-period spectrum, we may confirm the effectiveness of
293 partially self-centring steel frames compared with perfectly self-centring counterparts for
294 mitigating the structural seismic demands from an energy balance perspective. Therefore,
295 the concept of the hybrid energy dissipation bay equipped with SMA connections and
296 ductile links puts forth an engineering solution to realising various energy ratios in practice,
297 and the structural energy balance may be explicitly modulated.

298 To clearly demonstrate the influence of the hysteretic parameters on the mean energy
299 factor of partially self-centring SDF oscillators, the mean energy factor spectra of partially
300 self-centring SDF oscillators and perfectly self-centring counterparts with T = 0.1 s, 0.5 s,
301 1.0 s, 1.5 s, 2.0 s and 2.5 s are extracted from the analysis database, as shown in Fig. 6.
302 Thus, the dependency of the energy factor on hysteretic parameters is affirmed. According

303 to Fig. 6, it can be seen that an increasing energy ratio leads to substantial reduction of the
304 mean energy factor regardless of the hysteretic parameters, particularly for SDF systems in
305 the long period region. Hence, the beneficial effect of introducing the partially
306 self-centring behaviour into a steel frame is confirmed.
307
308 *4.2. Probabilistic properties of energy factor spectra*
309 For a representative SDF oscillator with specified hysteretic parameters (i.e.
310 post-yielding stiffness ratio, ductility factor and energy ratio), the probability distribution
311 of 320 energy factor can be obtained. For each combination of hysteretic parameters, fifty
312 probability histograms of the energy factor may be determined considering fifty vibration
313 periods. Representative illustrations are shown in Fig. 7. It is evident that an increasing
314 post-yielding stiffness ratio leads to a decreasing dispersion of the energy factor (Fig. 7a),
315 whereas an increasing target ductility factor increases the dispersion of the index (Fig. 7b).
316 This phenomenon is in line with energy factor spectra of bilinear kinematic SDF systems
317 according to a previous study [36]. In addition, it is seen that an increasing energy ratio
318 also appreciably influences the probability distribution of the energy factor, as shown in
319 Fig. 7c. It is worth noting that the statistic distribution of the energy factors exhibits an
320 evident asymmetry according to Fig. 7, and the skewness of the energy factor distribution
321 varies for a SDF system with varied vibration period and hysteretic parameters. For
322 instance, the skewness of the energy factor becomes more pronounced in cases with a
323 more significant target ductility factor. Comparatively, an increasing post-yielding
324 stiffness ratio mitigates this phenomenon. Thus, to reasonably characterise the energy

factor distribution of the SDF system representing damage-control steel frames equipped with SMA connections and ductile energy dissipation links exhibiting partially self-centring behaviour, an applicable spectral model accounting for the probabilistic characteristics of the energy factor may be desirable.

5. Spectral energy factor model

Compared with using the mean energy factor spectra [36, 37] for quantification of energy factor demands, spectral models considering the probabilistic characteristics of the energy factor may be more desirable as the statistic distribution of the index can be captured, and the attractiveness of quantifying structural inelastic seismic demand based on probabilistic models was echoed by recent research [38-40]. For the purpose of demonstration, histograms of energy factors with the vibration period ranging from 0.2 s to 3.0 s (i.e. T = 0.2 s, 0.4 s, 0.6 s, 0.8 s, 1.0 s, 1.5 s, 2.0 s, 2.5 s and 3.0 s) and a fixed hysteretic parameter combination (i.e. α = 0.5, μ = 3 and β = 0.8) are shown in Fig. 8. Note that the similar observation can be characterised for systems with other vibration periods and hysteretic parameters.

Because the lognormal distribution is generally applicable in describing the probabilistic features of inelastic seismic demands [38, 39], it was utilised as the basis for developing a spectral model for quantifying the seismic demand of damage-control steel frames equipped with SMA connection and ductile links. Specifically, the probability density function (PDF) of the energy factor with specified matrix of the vibration period and hysteretic parameters dominated by a lognormal distribution is given by

$$PDF(\Omega) = \frac{1}{\Omega} \cdot \frac{1}{\sqrt{2\pi}(\ln\gamma)_{s.dev}} \cdot \exp\left\{ -\frac{\left[\ln\Omega - (\ln\gamma)_{ave}\right]^2}{2\left[(\ln\gamma)_{s.dev}\right]^2} \right\} \quad (5)$$

where Ω = a possible value of the energy factor; $(\ln\gamma)_{ave}$ = the mean value of $\ln\gamma$ and $(\ln\gamma)_{s.dev}$ = standard deviation of $\ln\gamma$. To justify the sufficiency of the lognormal distribution model for featuring the probabilistic properties of the energy factor, probability density curves produced by Eq. (5) (i.e. red solid curves) are compared with the histograms of the energy factors shown in Fig. 8. Thus, the reasonable agreement between the energy factor distribution and predictions by the lognormal distribution model is seen.

From a practical application point of view, the spectral model of the energy factor based on the lognormal distribution assumption may be developed by confirming prediction equations of $(\ln\gamma)_{ave}$ and $(\ln\gamma)_{s.dev}$ according to Eq. (5). Recalling that both energy factor and the deviation are appreciably affected by the vibration period and hysteretic parameters, we may develop a spectral energy factor model by taking all influential parameters into account. In the current study, the nonlinear regression package Tablecurve 3D was utilised to perform a multi-step nonlinear regression analysis.

To initiate the nonlinear regression analyses, the relationship between $(\ln\gamma)_{ave}$ and the vibration period (T) for each combination of hysteretic parameters (i.e. α, β and μ) was first determined based on the energy factor database, and the following equation was finalised based on a trial-and-error procedure, given by:

$$(\ln\gamma)_{ave} = OT^P + Q \quad (6)$$

where O, P and Q are coefficients to be regressed. Similarly, the correlation between $(\ln\gamma)_{s.dev}$ and the vibration period (T) was developed, given by

$$\left(\ln\gamma\right)_{s.dev} = RT^2 + ST + U \tag{7}$$

where R, S and U are the regressed coefficients. It is worth noting that the two equations were selected from more than 450 million built-in formulas in the programme. Both computational accuracy and practical simplicity were taken into account when choosing the format of the equations. Representative $(\ln\gamma)_{ave}$-T relationship and $(\ln\gamma)_{s.dev}$-T relationship are compared with predictions by the equations, as shown in Fig. 9 and Fig. 10, respectively, and the satisfactory accuracy of the equation for capturing the general trend of $(\ln\gamma)_{ave}$ and $(\ln\gamma)_{s.dev}$ is seen.

Then, the influence of the hysteretic parameters governing the skeleton response was considered, and the regressed coefficients (i.e. O, P, Q, R, S and U) were rearranged and expressed by

$$O = F_O(\alpha,\mu) = \exp\left(O_1 + O_2\alpha + \frac{O_3}{\mu}\right) \tag{8}$$

$$P = F_P(\alpha,\mu) = P_1 + P_2\alpha^{0.5} + \frac{P_3}{\mu^{0.5}} \tag{9}$$

$$Q = F_Q(\alpha,\mu) = \frac{1}{Q_1 + Q_2\alpha^{1.5} + \frac{Q_3}{\ln(\mu)}} \tag{10}$$

$$R = F_R(\alpha,\mu) = \frac{1}{R_1 + R_2\alpha^{3} + \frac{R_3}{\ln(\mu)}} \tag{11}$$

$$S = F_S(\alpha,\mu) = \frac{1}{S_1 + S_2\alpha^{3} + \frac{S_3}{\ln(\mu)}} \tag{12}$$

$$U = F_U(\alpha,\mu) = \frac{1}{U_1 + U_2\alpha \ + \frac{U_3}{\ln(\mu)}} \tag{13}$$

where O_i, P_i, Q_i, R_i, S_i and U_i were further correlated with the energy ratio (β) controlling

386 the partially self-centring behaviour, and given by

387 $$O_1 = -0.450\beta^2 + 0.067\beta + 1.446 \quad (14)$$

388 $$O_2 = -1.375\beta^2 + 1.669\beta - 3.358 \quad (15)$$

389 $$O_3 = 6.075\beta^2 - 6.935\beta - 6.465 \quad (16)$$

390 $$P_1 = -0.125\beta^2 + 0.455\beta - 0.079 \quad (17)$$

391 $$P_2 = -0.650\beta^2 + 0.475\beta - 0.278 \quad (18)$$

392 $$P_3 = 1.450\beta^2 - 2.837\beta - 0.374 \quad (19)$$

393 $$Q_1 = 0.825\beta^2 - 1.662\beta + 1.130 \quad (20)$$

394 $$Q_2 = 0.550\beta^2 + 0.283\beta - 3.463 \quad (21)$$

395 $$Q_3 = -1.900\beta^2 + 3.722\beta - 3.414 \quad (22)$$

396 $$R_1 = 110.300\beta^2 - 127.200\beta + 52.900 \quad (23)$$

397 $$R_2 = -244.500\beta^2 + 914.400\beta - 993.000 \quad (24)$$

398 $$R_3 = -264.100\beta^2 + 263.300\beta - 154.000 \quad (25)$$

399 $$S_1 = -7.150\beta^2 - 1.405\beta - 2.706 \quad (26)$$

400 $$S_2 = 109.200\beta^2 - 289.700\beta + 260.700 \quad (27)$$

401 $$S_3 = 25.720\beta^2 + 8.930\beta + 12.340 \quad (28)$$

402 $$U_1 = 0.275\beta^2 - 0.238\beta + 0.488 \quad (29)$$

403 $$U_2 = -2.000\beta^2 + 2.774\beta + 0.564 \quad (30)$$

404 $$U_3 = 0.700\beta^2 - 1.460\beta + 2.189 \quad (31)$$

405 During the regression procedure, the convergence of the iterations was governed by the
406 least square principle. To demonstrate the accuracy of the spectral energy factor model, the
407 PDFs based on the proposed equations were also shown in Fig. 8 (Dash lines), and the

accuracy of the model for capturing the probabilistic characteristics of the energy factor can be confirmed.

In this context, the cumulative distribution function (CDF) of the energy factor could be obtained, given by

$$\mathrm{CDF}(\Omega) = \Phi\left[\frac{\ln\Omega - (\ln\gamma)_{\mathrm{ave}}}{(\ln\gamma)_{\mathrm{s.dev}}}\right] = \Phi\left[\frac{\ln\Omega - (OT^{P} + Q)}{RT^{2} + ST + U}\right] \quad (32)$$

where Φ = CDF of the standard normal distribution. Hence, based on the seismic energy factor of the system, the damage-control behaviour of steel frame equipped with SMA connections and ductile links considering probabilistic characteristics can be evaluated, which will be discussed in the later section.

6. Application of the spectral energy factor model in damage-control evaluation of steel frames equipped with SMA connections and ductile links

6.1. Stepwise damage-control evaluation procedure based on the spectral energy factor model

Based on the spectral model, a stepwise damage-control evaluation procedure for the novel structure dominated by the fundamental vibration mode was proposed and given as follows:

Step 1: Conduct frequency analysis and compute the elastic vibration characteristics of a structure including the vibration period (T), the effective mass (M^{*}), and the modal vector ($\boldsymbol{\varphi}_1$).

Step 2: Perform cyclic pushover analysis considering the fundamental mode and confirm the hysteretic parameters along with the damage-control threshold (e.g. roof drift

threshold). It was worth noting that data fitting approach may be used to quantify the hysteretic parameters by multilinear simplification.

Step 3: Idealise the structure as an equivalent SDF system considering the fundamental mode, and develop the "energy-based pushover response curve" as well as the "nominal energy capacity response curve" for the SDF system. In particular, the nominal energy capacity response may be produced based on the skeleton pushover responses, and it quantifies the absorbed energy of the system under the pushover loads. According to the energy equilibrium, the nominal energy capacity curve can be generated by calculating the work done by the lateral pushover loads. The detailed information about the method motivated by an incremental approach was proposed by Hernandez-Montes et al. [41].

Step 4: Set the performance target and generate the probabilistic energy demand curves. In particular, based on the preselected pseudo spectral acceleration demand (S_a) under which the structural damage-control behaviour should be achieved, the nominal energy demand curve may be determined by the following:

$$E_{\mathrm{d}} = \frac{M^{*} g^{2} T^{2}}{8\pi^{2}} \bar{\gamma}\left(\alpha, \mu, \beta\right) S_a^2 \tag{33}$$

$$CDF\ (\bar{\gamma}) = \Phi\left[\frac{\ln \bar{\gamma} - \left(OT^{P} + Q\right)}{RT^{2} + ST + U}\right] > \Theta \tag{34}$$

where g = gravity acceleration, $\bar{\gamma}\left(\alpha, \mu, \beta\right)$ = energy factor threshold and Θ = predefined performance target.

Step 5: Arrange the probabilistic energy demand curves and the nominal energy capacity curve in one diagram. The probabilistic performance point may be determined by the intersection point of the probabilistic energy demand curve and the corresponding

451 energy capacity curve. In this context, the damage-control evaluation can be conducted by
452 comparing the predefined damage-control threshold and the intersection point.
453
454 *6.2. Information about prototype structure*
455 A prototype system designated as office building was developed to examine the
456 effectiveness of the spectral energy factor model for quantifying the structural
457 damage-control behaviour. Fig. 11a and Fig. 11b present the layout and elevation of the
458 three-storey office building, respectively, and the emphasis of this study is given to a 2-D
459 frame as indicated in Fig. 11a. For the prototype system, the dead load and live load were
460 assumed as 5 kN/m^2 and 2.5 kN/m^2, respectively, which was in line with the Chinese load
461 code for design of building structures (GB50009-2012) [42]. The seismic weight and
462 gravity load of the 2-D frame were determined by the tributary area indicated in Fig. 11a.
463 The elastic seismic design was conducted according to Chinese design provisions
464 GB50011-2010 (2016) [43].
465 To realise the expected damage-control behaviour by limiting inelastic actions in the
466 SMA connections and ductile links, the main frame was composed Q460 high strength
467 steel members with nominal yield strength of 460 MPa (Fig. 11b). Two "hybrid energy
468 dissipation bays" equipped with SMA connections and ductile links were placed at the
469 external bays of the frame, as schematically shown in Fig. 11b. In particular, the H-shaped
470 Q235 mild carbon steel links and self-centring links with the SMA connections were
471 installed in the hybrid energy dissipation bays. The detailed configuration of the SMA
472 connections is shown in Fig. 12. For all SMA connections, HS bolts with four SMA

washers were implemented. The detail of the HS bolts with SMA washers was consistent with the "W8" configurations in the previous experimental study done by Yam and colleagues [14]. To enlarge the elastic deformation range of the main frame, pin connections were utilised to connect the high strength steel beams with the "hybrid energy dissipation bays" (Fig. 11b). By employing pinned connections in the main frame, the rotation of the beam at one end of the beam can be released, and hence the deformation pattern of the beam in the main frame can be changed. Consequently, the yield drift of the main frame can be enlarged. In addition, to trigger simultaneous inelasticity inception of the SMA connections and ductile links, nonlinear pushover analysis was used in the design phase to optimise the structural design, and an iterative procedure was adopted. The length of the SMA bars (L) was set as 300 mm and 250 mm for the first two floors and the roof floor, respectively. The distance of the SMA bars (S) was set as 550 mm, 600 mm and 450 mm considering the first floor, the second floor and the roof floor, respectively. The modelling detail will be discussed and verified in the next subsection.

6.3. Modelling techniques and verifications

The finite element (FE) package ABAQUS [44] was adopted to develop the analysis model of the prototype system. Linear beam elements (i.e. B31 elements) were used to model columns and the beams in the frame structure. The general mesh size for regions away from the inelastic action region was set as 250 mm, and the sizes of the mesh for the "plastic region" was refined. The bilinear kinematic model governed by the von Mises yield criterion was used for Q460 high strength steel members and ductile links. The adequacy of

the modelling techniques for simulating the hysteretic behaviour of Q460 high strength steel members and ductile links was justified in recent research works [36, 45]. The test data of a steel frame composed of Q460 high strength steel members and ductile links made from Q235 steel are compared with predictions by the FE models, as shown in **Appendix A**.

As for the SMA connection, a simplified numerical model was developed, as schematically shown in Fig. 13a. Specifically, nonlinear truss element assigned with the Auricchio's hysteretic material model [46] were utilised to reproduce the behaviour of the superelastic SMA bolts, and rigid elements were used to simulate the effect of the "Steel washer". Thus, the length of the truss elements was identical to the gauge length of the bolt in the connection. Because the connection was able to offer sufficient shear rigidity, as was confirmed in the previous test programme [14], the shear flexibility of the connection was neglected. This was realised by connecting the column and the endplate with a rigid shear spring element. Likewise, the effect of SMA Belleville washers was simulated by a nonlinear truss element. The essential material parameters of the superelastic SMA including the forward transformation start stress (σ^{MS}), the forward transformation end stress (σ^{Mf}), the reverse transformation start stress (σ^{AS}), the reverse transformation end stress (σ^{Af}), austenite elasticity (E^{A}), martensite elasticity (E^{M}), maximum transformation strain (ε^{L}), and Poisson ratios (ν^{A} and ν^{M}) are summarised in Table 1. These material properties were determined based on the coupon tests results reported by Yam's group [14]. The material model of the SMA based on Fang et al. [14] is reproduced in Fig. 13b. The FE modelling techniques of the SMA connection were applied to model test connections examined by Yam and colleagues (i.e. specimen D8L240 and D8L290W8) [14], and the FE predictions

517 are plotted against test responses, as shown in Fig. 14. The reasonable agreement between
518 the test results and the FE predictions confirmed the sufficiency of the simplified connection
519 model for reproducing the hysteretic behaviour of the SMA connection. In this paper, the
520 SMA connection (D8L290W8), which had higher connection resistance and stiffness
521 compared with the counterpart without HS bolts and SMA washers, was introduced to
522 enhance the seismic performance of the prototype structure. In this context, the modelling
523 techniques were utilised to develop the prototype structure. The elastic dynamic properties
524 of the prototype structure are extracted and shown in Table 2.

525

526 *6.4. Validation of the structural hysteretic model*

527 To examine the feasibility of the structural hysteretic model for characterising the cyclic
528 response of the novel structure, nonlinear cyclic pushover analysis was performed. The
529 invariant lateral pushover load pattern being consistent with the fundamental vibration mode
530 was applied on the prototype structure. The results in terms of the base shear versus roof
531 drift responses were extracted from the analysis database and correlated with the
532 simplification by the partially self-centring hysteretic model (Fig. 2), as shown in Fig. 15.
533 The solid blue line is the hysteretic model path representing the partially self-centring
534 system. A good agreement between the analysis results and the model simplification was
535 characterised, and the adequacy of using the hysteretic model for quantifying the energy
536 factor of damage-control steel frames equipped with SMA connections and ductile links can
537 be confirmed.

538

539 *6.5. Validation of the spectral energy factor model for damage-control evaluations*

To demonstrate the effectiveness of the energy factor model for quantifying the damage-control behaviour of a steel frame equipped with SMA connections and ductile links showing the partially self-centring behaviour, a validation study was carried out. According to the pushover analysis database, the column in the main frame began to yield when the roof drift reached 3%. Thus, the roof drift of 3% was set as the damage-control threshold. As a case study, S_a (T_1) = 0.6 g was randomly selected as a predefined seismic intensity level. Based on the equivalent SDF system of the prototype structure (i.e. the inelastic SDF system with the effective mass and the period corresponding to the fundamental vibration mode), the predicted energy factor curves with varied performance targets (i.e. Θ) are shown in Fig. 16a. In the figure, the probabilistic energy factor corresponding to the CDF of 99%, 85%, 75%, 50% are plotted against the ductility factor. The probability distribution of the energy factor of the representative SDF system under 320 earthquake motions are also demonstrated in Fig. 16a. It is interesting but important to note that the correlation between the energy factor and the ductility factor was dependent on the performance target. In cases with Θ = 50%, 75% and 85%, the energy factor generally decreases with an increasing ductility factor. When Θ was set as 99%, the energy factor increases with increasing ductility factor. The energy demand curves corresponding to various performance targets Θ were computed based on Eqs. (33) and (34), and they are correlated with the energy capacity curves, as shown in Fig. 16b. It is seen that the intersections between all energy demand curves and the energy capacity curves can be achieved before the deformation going beyond the predefined threshold in case of S_a =0.6 g. Therefore, it may be expected that the prototype structure can achieve the

562 damage-control behaviour rigorously with S_a =0.6 g.

563 To examine the robustness of the proposed model, nonlinear response history analyses
564 were performed using thirty near-field earthquake records. The thirty additional earthquake
565 motions were downloaded from PEER [31] or extracted from the SAC earthquake
566 database [47], and they were not in the earthquake database examined in Section 3. The
567 detailed information about the additional thirty earthquakes is shown in Table 3. Thus, the
568 earthquake motions were scaled to a spectral acceleration S_a = 0.6 g at the period of 0.83 s
569 (i.e. the fundamental period of the prototype structure). In the analyses, the Rayleigh
570 damping assumption was used, and the damping ratio of 5% for the first two vibration
571 modes was used to develop the damping matrix. The maximum interstorey drift responses
572 of the prototype structure subjected to earthquake motions were shown in Fig. 17a, and the
573 interstorey drift corresponding to the predefined resilience threshold (roof drift = 3%) is
574 also indicated in the figure. Therefore, it can be confirmed that the prototype system
575 deformed in the damage-control stage under the thirty earthquake motions, and the
576 adequacy of the energy factor model was justified. The post-earthquake residual drift was
577 also extracted and shown in Fig. 17b, and additional 100 s were considered in the analysis
578 to allow for vibration decaying. As can be seen, the post-residual drift was insignificant,
579 which was much lower than 0.5% reckoned as the resilience threshold of a structure [2].
580 Therefore, the great potential of steel frames equipped with SMA connections and ductile
581 links as a seismic resilient structure is apparent.

582

583 *6.6. Further analyses and discussions*

584 For the partially self-centring steel frames equipped with SMA connections and ductile
585 links, the enhanced energy dissipation capacity is realised at the expense of the recentring
586 ability. To examine the influence of this factor, further comparative analyses of the
587 partially self-centring SDF systems representing the proposed prototype structure and that
588 of perfectly flag-shaped SDF systems representing conventional self-centring steel frames
589 were performed. To further confirm the rationality that a low-to-medium rise steel frame
590 can be idealised by an equivalent SDF system for seismic response estimation [22], the roof
591 displacement history responses of the proposed prototype structure and that derived from
592 the equivalent SDF system considering the fundamental vibration mode of the structure [22]
593 under a ground motion randomly selected from the earthquake database (N11 in Table 3)
594 were compared, as shown in Fig. 18a. The good agreement between the roof displacement
595 history responses of the proposed prototype structure and that of the equivalent SDF system
596 is seen. Therefore, the yield strength and elastic vibration properties corresponding to the
597 fundamental vibration mode of the proposed prototype structure were assigned to inelastic
598 SDF systems, whilst the hysteretic parameters (i.e. post-yielding stiffness ratio and energy
599 ratio) were varied to shed lights on the "trade-off" between the energy dissipation capacity
600 and the recentring ability.
601 The mean residual displacement of the representative SDF system considering a spectrum
602 of hysteretic parameters under 320 earthquake motions is shown in Fig. 18b. As expected,
603 the post-yielding stiffness ratio (α) and the energy ratio (β) appreciably affect the mean
604 residual displacement of the SDF systems. For partially self-centring SDF systems ($\beta > 0.5$),
605 the residual displacement increases with increasing β. Nonetheless, the mean residual

606 displacement is still insignificant in cases where $0.5 < \beta \leq 0.7$. In cases where β goes beyond
607 0.7, a drastic increase of the mean residual displacement of partially self-centring SDF
608 systems was seen, whereas an increasing post-yielding stiffness ratio contributes to
609 suppressing this trend. Recalling that a significant post-yielding stiffness ratio can be
610 achieved by the elastic behaviour of high strength steel (HSS) frame members (Fig. 15) in
611 the main frame, the optimal seismic performance of the proposed partially self-centring steel
612 frame can be achieved by adjusting hysteretic parameters, and a reasonable balance between
613 the recentring ability and the energy dissipation capacity can be realised. The advantages of
614 increasing energy dissipation in a self-centring system and making the trade-off between
615 the recentring ability and the energy dissipation capacity of the structure are also echoed by
616 research findings in the literature [18, 48, 49].
617
618 **7. Summary and conclusions**

619 Recognising the limitations of conventional steel frames under seismic loading
620 scenarios, this research proposed the notion of damage-control steel frames equipped with
621 shape memory alloy (SMA) connections and ductile links showing the partially
622 self-centring behaviour. To shed insightful lights on the inelastic seismic demand of the
623 novel structure subjected to near-field earthquake motions, this paper explored a spectral
624 energy factor model which may be used to prescribe the structural peak inelastic seismic
625 demands. It is worth noting that the hysteretic model is applicable for a structure
626 deforming in the damage-control stage where the main frame members remain generally
627 elastic. In addition, the feasibility of the prototype structure was confirmed, whereas the

628 optimization of SMA connection and structure needs further examination.

629 In general, the hysteretic behaviour of steel frame equipped with SMA connections and
630 ductile links deforming in the damage-control stage can be characterised by a bilinear
631 partially self-centring hysteretic model, and the post-yielding stiffness ratio, ductility
632 factor and the energy ratio all appreciably affect the energy factor demand of the systems.
633 Utilising the single-degree-of-freedom (SDF) analogy, constant-ductility-based spectral
634 analyses were performed, and more than 25 million energy factors were gathered based on
635 an earthquake database with 320 near-field earthquake motions and a parameter matrix
636 covering a wide spectrum of parameters. According to the result database, it was
637 confirmed that an increasing post-yielding stiffness ratio may lead to a decreasing mean
638 energy factor for short-period partially self-centring SDF systems (T < 0.5 s), but the
639 opposite correlation between the energy factor and the post-yielding stiffness ratio was
640 characterised for systems falling in the longer period region. In contrast, the results showed
641 that an increasing ductility factor leads to an increasing mean energy factor for
642 short-period SDF systems, whereas the reversed trend was seen for systems with longer
643 period. The results also showed that an increasing energy ratio may lead to reduction of the
644 energy factor, which was more evident for long-period systems. Therefore, the rationale of
645 developing the partially self-centring steel frames to resist attacks of near-field earthquake
646 motions was confirmed.

647 By examining the probabilistic characteristics of the energy factors, we observed that
648 the energy factor of the partially self-centring steel frames equipped with SMA
649 connections and ductile links follows a right-skewed distribution. Thus, the lognormal

650 distribution model was used to replicate the statistic characteristics of the energy factors.
651 The good agreement between the energy factor data and the probability density function
652 curves based on the lognormal distribution model confirmed the adequacy of the
653 presumption. Therefore, a probabilistic spectral energy factor model for quantifying the
654 energy factor of a partially self-centring steel frame equipped with SMA connections and
655 ductile links deforming in the damage-control stage was developed using nonlinear
656 regression analyses, and the damage-control behaviour evaluation of the structure may be
657 conducted from a statistic perspective. The sufficiency of the energy factor model was
658 justified by using a prototype structure. In summary, the spectral energy factor model
659 blazed a path for damage-control evaluation considering varied performance targets, and
660 practitioners could conduct the design or evaluation of the novel steel frames efficiently
661 with the assistance of the model. In addition, the seismic responses of equivalent SDF
662 systems were further analysed, and the rationality of developing the partially self-centring
663 steel frames was confirmed.

664 It is worth noting that the focus of the current study was given to the spectral energy
665 factor, and the estimated seismic demand was conditional based on a predefined
666 pseudo-acceleration. A full-fledged probabilistic seismic demand model for partially
667 self-centring steel frames equipped with SMA connections and ductile links may be
668 developed based on a seismic hazard model quantifying the probabilistic characteristics of
669 seismic intensities (i.e. S_a), which is currently being conducted by the authors. In addition,
670 the proposed model may be limited to low-to-medium rise structures dominated by the
671 fundamental mode. In addition, steel frames equipped with shape memory alloy (SMA)

672 connections and ductile links deforming in the damage-control stage were emphasised,
673 whereas the behaviour of the system in the post-damage-control stage with inelasticity
674 spreading to the main frame needs further efforts.

675

676 **Appendix A**

677 The comparison between the moment responses of Q460 high strength steel members and
678 Q235 ductile links from a recent test programme [45] and FE predictions based on the
679 modelling techniques is reproduced in Fig. A1.

680

681 **Figure captions**

682 Fig. 1 Damage-control steel frame equipped with SMA connections and ductile links in
683 hybrid energy dissipation bays: (a) structural concept and (b) deformed pattern of the SMA
684 connection under hogging action [14].

685 Fig. 2 Hysteretic model.

686 Fig. 3 Definition of the energy factor.

687 Fig. 4 320 earthquake motions.

688 Fig. 5 Representative mean energy factor spectra.

689 Fig. 6 Influence of hysteretic parameters on the mean energy factor.

690 Fig. 7 Influence of hysteretic parameters on the dispersion of the energy factor.

691 Fig. 8 Representative histograms and the corresponding probability density function
692 curves of the energy factor.

693 Fig. 9 Representative $(\ln \gamma)_{ave}$ - T spectra.

694 Fig. 10 Representative $(\ln \gamma)_{s,dev}$ - T spectra.

695 Fig. 11 Information on the prototype structure.

696 Fig. 12 Configuration of the SMA connections.

697 Fig. 13 Simplified SMA connection model and material characteristics: (a) simplified
698 model and (b) material model.

699 Fig. 14 Verification of the simplified connection model.

700 Fig. 15 Verification of the structural hysteretic model.

701 Fig. 16 Probabilistic energy demand curves and capacity curves: (a) probabilistic energy
702 factor spectra and (b) damage-control evaluation diagram.

703 Fig. 17 Analysis results by NL-RHA: (a) Peak interstorey drift and (b) residual interstorey
704 drift.

705 Fig. 18 Seismic responses of the equivalent SDF system: (a) the roof displacement history
706 responses and (b) the mean residual displacement responses.

707 Fig. A1 Validation of the modelling techniques of main frame members and ductile links.

708

709 **Acknowledgements**

710 This research is financially supported by the National Natural Science Foundation of
711 China (Grant No. 51890902 and 51708197) and the Research Grants Council of the Hong
712 Kong Special Administrative Region, China with Grant No. PolyU 152096/19E. Partial
713 funding supports from Chinese National Engineering Research Centre for Steel
714 construction, The Hong Kong Polytechnic University (Project No. 1-BBV4) are also
715 gratefully acknowledged. The corresponding author is truly appreciative of the constant

716 support from his beloved wife Siqin, his daughter Yutong and all his families in this hard
717 period.

718

719 **References**

720 [1] Okazaki T, Lignos DG, Midorikawa M, Ricles JM, Love J. Damage to steel buildings
721 observed after the 2011 Tohoku-Oki earthquake. Earthq Spectra 2013; 29(S1): S219-
722 S243.
723 [2] Erochko J, Christopoulos C, Tremblay R, Choi H. Residual drift response of SMRFs and
724 BRB frames in steel buildings designed according to ASCE 7-05. J Struct Eng 2011;
725 137(5): 589-599.
726 [3] Zhang AL, Zhang YX, Li R, Wang ZY. Cyclic behavior of a prefabricated self-centering
727 beam-column connection with a bolted web friction device. Eng Struct 2016; 111:
728 185-198.
729 [4] Garlock MM, Sause R, Ricles JM. Behavior and design of posttensioned steel frame
730 systems. J Struct Eng 2007; 133(3): 389-399.
731 [5] Christopoulos C, Tremblay R, Kim HJ, Lacerte M. Self-centering energy dissipative
732 bracing system for the seismic resistance of structures: development and validation. J
733 Struct Eng 2008; 134(1): 96-107.
734 [6] Deogekar PS, Andrawes B. Probabilistic seismic demand models for shape memory
735 alloy retrofitted RC bridge columns. J Bridge Eng 2018; 23(8): 04018050.
736 [7] Ghafoori E, Neuenschwander M, Shahverdi M, Czaderski C, Fontana M. Elevated
737 temperature behavior of an iron-based shape memory alloy used for prestressed
738 strengthening of civil structures. Constr Build Mater 2019; 211: 437-452.
739 [8] Wang B, Zhu S, Casciati F. Experimental study of novel self-centering seismic base
740 isolators incorporating superelastic shape memory alloys. J Struct Eng 2020; 146(7):

741 04020129.
742 [9] Wang B, Zhu S, Chen K, Huang J. Development of superelastic SMA angles as
743 seismic-resistant self-centering devices. Eng Struct 2020; 218: 110836.
744 [10] Wang B, Zhu S. Cyclic tension-compression behavior of superelastic shape memory
745 alloy bars with buckling-restrained devices. Constr Build Mater 2018; 186: 103- 113.
746 [11] Wang B, Zhu SY. Superelastic SMA U-shaped dampers with self-centering functions.
747 Smart Mater Struct 2018; 27(5): 055003.
748 [12] Ocel J, DesRoches R, Leon RT, Hess WG. Steel beam-column connections using shape
749 memory alloys. J Struct Eng 2004; 130(5): 732-740.
750 [13] Fang C, Yam MCH, Lam ACC, Xie LK. Cyclic performance of extended end-plate
751 connections equipped with shape memory alloy bolts. J Constr Steel Res 2014; 94:
752 122-136.
753 [14] Fang C, Yam MCH, Chan TM, Wang W, Yang X, Lin X. A study of hybrid self-centring
754 connections equipped with shape memory alloy washers and bolts. Eng Struct 2017;
755 164: 155-168.
756 [15] Wang B, Zhu S, Qiu C X, Jin H. High-performance self-centering steel columns with
757 shape memory alloy bolts: Design procedure and experimental evaluation. Eng Struct
758 2019; 182: 446-458.
759 [16] DesRoches R, Taftali B, Ellingwood BR. Seismic performance assessment of steel
760 frames with shape memory alloy connections. Part I-Analysis and seismic demands. J
761 Earthquake Eng 2010; 14(4): 471-486.
762 [17] Sultana P, Youssef MA. Seismic performance of steel moment resisting frames utilizing
763 superelastic shape memory alloys. J Constr Steel Res 2016; 125: 239- 251.
764 [18] Christopoulos C, Filiatrault A, Folz B. Seismic response of self-centring hysteretic
765 SDOF systems. Earthq Eng Struct Dyn 2002; 31(5): 1131-1150.

766 [19] Zhang C, Steele TC, Wiebe LDA. Design-level estimation of seismic displacements for
767 self-centering SDOF systems on stiff soil. Eng Struct 2018; 177: 431-443.
768 [20] Housner GW. Limit design of structures to resist earthquakes. Proceeding of the 1st
769 World Conference on Earthquake Engineering 1956.
770 [21] Lee SS, Goel SC, Chao SH. Performance-based design of steel moment frames using a
771 target drift and yield mechanism. Research Report No. UMCEE 01-17, Dept. of Civil
772 and Envr. Engr., Univ. of Michigan, Ann Arbor, MI. 2001.
773 [22] Leelataviwat S, Saewon W, Goel SC. Application of energy balance concept in seismic
774 evaluation of structures. J Struct Eng 2009; 135(2): 113-121.
775 [23] Ke K, Yam MCH, Zhang H, Lam ACC, Zhou X. High strength steel frames with SMA
776 connections in self-centring energy dissipation bays: behaviour insights and a
777 multi-mode-based nonlinear static procedure. Smart Mater Struct 2020; 29:125020.
778 [24] Qiu CX, Zhu S. Performance-based seismic design of self-centering steel frames with
779 SMA-based braces. Eng Struct 2017; 130: 67-82.
780 [25] Zhou Y, Song G, Huang S, Wu H. Input energy spectra for self-centering SDOF systems.
781 Soil Dyn Earthq Eng 2019; 121: 293-305.
782 [26] Zhou Y, Song G, Tan P. Hysteretic energy demand for self-centering SDOF systems.
783 Soil Dyn Earthq Eng 2019; 125: 105703.
784 [27] Shen Y L, Christopoulos C, Mansour N, Tremblay R. Seismic design and performance
785 of steel moment-resisting frames with nonlinear replaceable links. J Struct Eng 2011;
786 137(10): 1107-1117.
787 [28] Mansour N, Christopoulos C, Tremblay R. Experimental validation of replaceable
788 shear links for eccentrically braced steel frames. J Struct Eng 2011; 137(10): 1141-1152.
789 [29] Ke K, Yam MCH. A performance-based damage-control design procedure of hybrid
790 steel MRFs with EDBs. J Constr Steel Res 2018; 143: 46-61.

[30] Zhai C, Ji D, Wen W, Lei W, Xie L. Constant ductility energy factors for the near-fault pulse-like ground motions. J Earthq Eng 2016; 21(2): 343-358.

[31] Center PEER. Pacific Earthquake Engineering Research Center. PEER strong motion database. < https://ngawest2.berkeley.edu/ >

[32] Hatzigeorgiou GD. Ductility demand spectra for multiple near-and far-fault earthquakes. Soil Dyn Earthq Eng 2010; 30(4): 170-183.

[33] Dabaghi M. Stochastic modeling and simulation of near-fault ground motions for performance-based earthquake engineering. UC Berkeley, 2014.

[34] Vargas R, Bruneau M. Experimental response of buildings designed with metallic structural fuses. II. J Struct Eng 2009; 135(4): 394-403.

[35] Ke K, Wang W, Yam MCH, Deng L. Residual displacement ratio demand of oscillators representing HSSF-EDBs subjected to near-fault earthquake ground motions. Eng Struct 2019; 191: 598-610.

[36] Ke K, Yam MCH, Ke S. A dual-energy-demand-indices-based evaluation procedure of damage-control frame structures with energy dissipation fuses. Soil Dyn Earthq Eng 2017; 95: 61-82.

[37] Ke K, Zhao Q, Yam MC, Ke S. Energy factors of trilinear SDOF systems representing damage-control buildings with energy dissipation fuses subjected to near-fault earthquakes. Soil Dyn Earthq Eng 2018; 107: 20-34.

[38] Xiang Y, Luo YF, Huang Q L, Zhu ZC. Probabilistic inelastic seismic demand spectra for large-span planar steel structures subjected to vertical ground motions. Eng Struct 2018; 174: 646-662.

[39] Xiang Y, Koetaka Y. Ductility demand of bilinear hysteretic systems with large post-yield stiffness: Spectral model and application in the seismic design of dual-systems. Eng Struct 2019; 187: 504-517.

816 [40] Guo JWW, Christopoulos C. A probabilistic framework for estimating the residual drift
817 of idealized SDOF systems of non- degrading conventional and damped structures.
818 Earthq Eng Struct Dyn 2018; 47(2): 479-496.
819 [41] Hernandez-Montes E, Kwon OS, Aschheim MA. An energy-based formulation for
820 first- and multiple-mode nonlinear static (pushover) analyses. J Earthq Eng 2004; 8(1):
821 69-88.
822 [42] GB50009-2012. Load code for Design of Buildings (GB50009-2012). Chinese
823 Building Press, Beijing, China; 2012.
824 [43] GB50011-2010. Code for Seismic Design of Buildings (GB50011-2010). Chinese
825 Building Press, Beijing, China; 2010.
826 [44] ABAQUS Analysis User's Manual. ABAQUS Standard, Version 6.12; 2012.
827 [45] Ke K, Yam MCH, Deng L, Zhao Q. A modified DEB procedure for estimating seismic
828 demands of multi-mode-sensitive damage-control HSSF-EDBs. J Constr Steel Res 2018;
829 150: 329-345.
830 [46] Auricchio F, Coda A, Reali A, Urbano M. SMA numerical modeling versus
831 experimental results: parameter identification and model prediction capabilities. J
832 Mater Eng Perform 2009; 18(5-6): 649-54.
833 [47] Somerville P. Development of ground motion time histories for phase 2 of the
834 FEMA/SAC steel project, SAC Background Document SAC/BD-91/04. Sacramento,
835 Calif: SAC Joint Venture, 1997.
836 [48] Qiu CX, Zhu S. High-mode effects on seismic performance of multi-story
837 self-centering braced steel frames. J Constr Steel Res 2016; 119: 133–43.
838 [49] Fang C, Zhong Q, Wang W, Hu S, Qiu CX. Peak and residual responses of steel
839 moment-resisting and braced frames under pulse-like near-fault earthquakes. Eng Struct
840 2018; 177: 579-597.

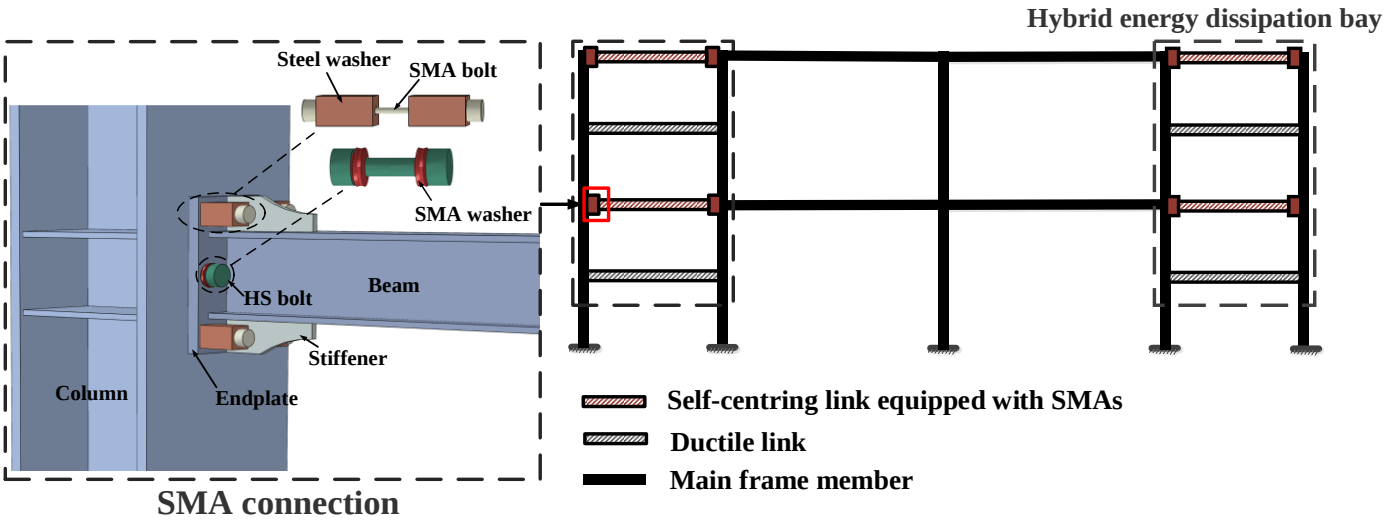

(a)

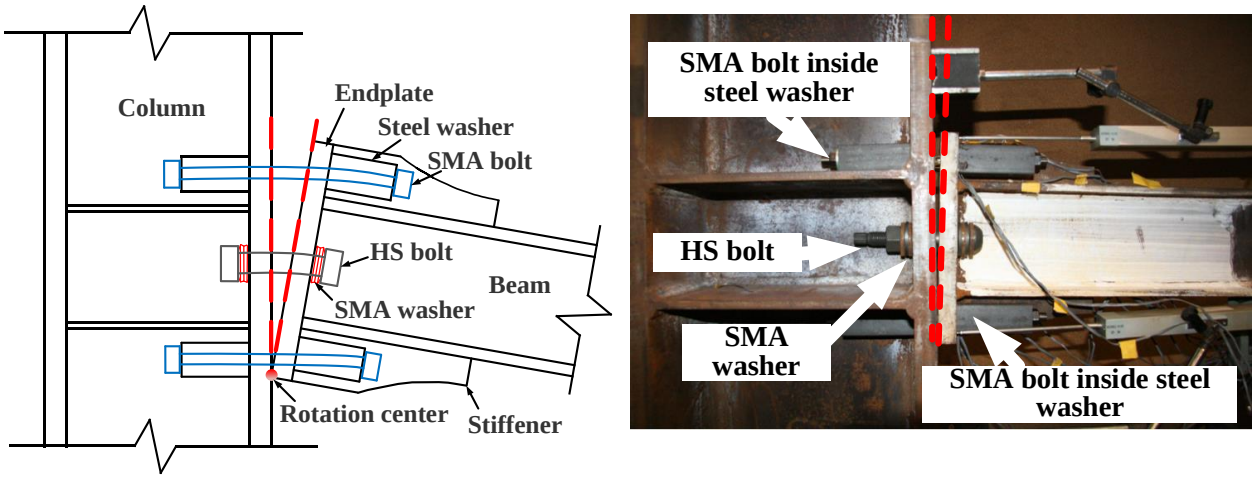

(b)

Fig. 1 Damage-control steel frame equipped with SMA connections and ductile links in hybrid energy dissipation bays: (a) structural concept and (b) deformed pattern of the SMA connection under hogging action [14].

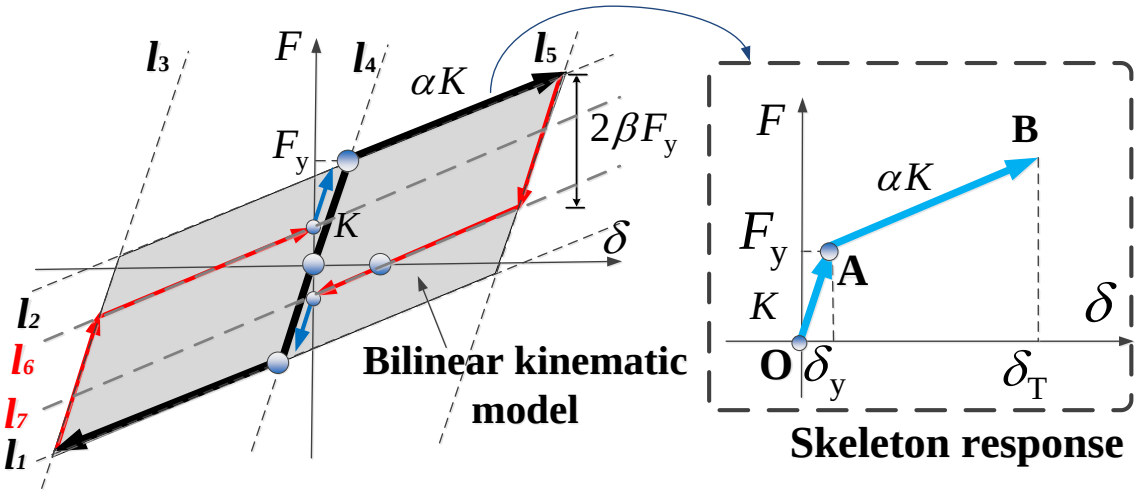

Fig. 2 Hysteretic model.

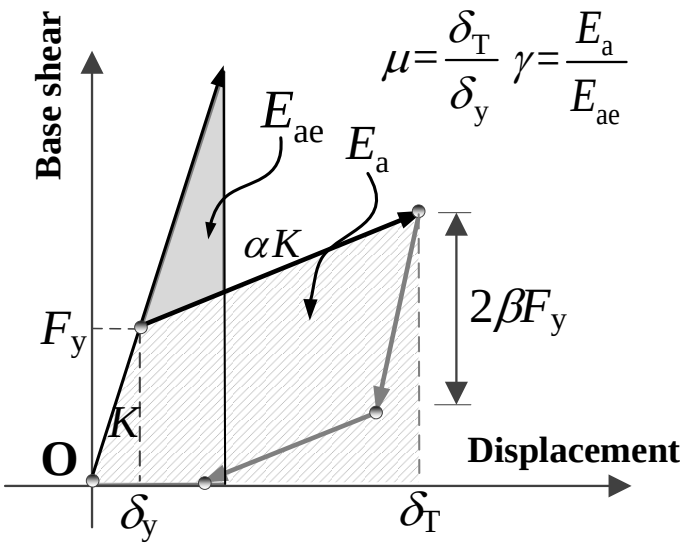

Fig. 3 Definition of the energy factor.

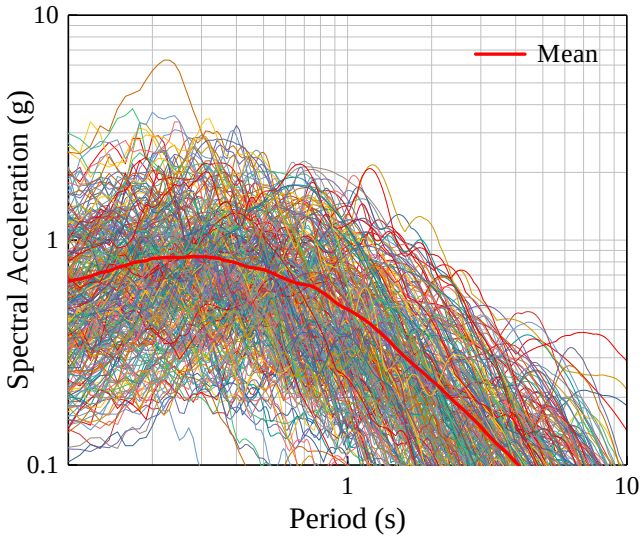

Fig. 4 320 earthquake motions.

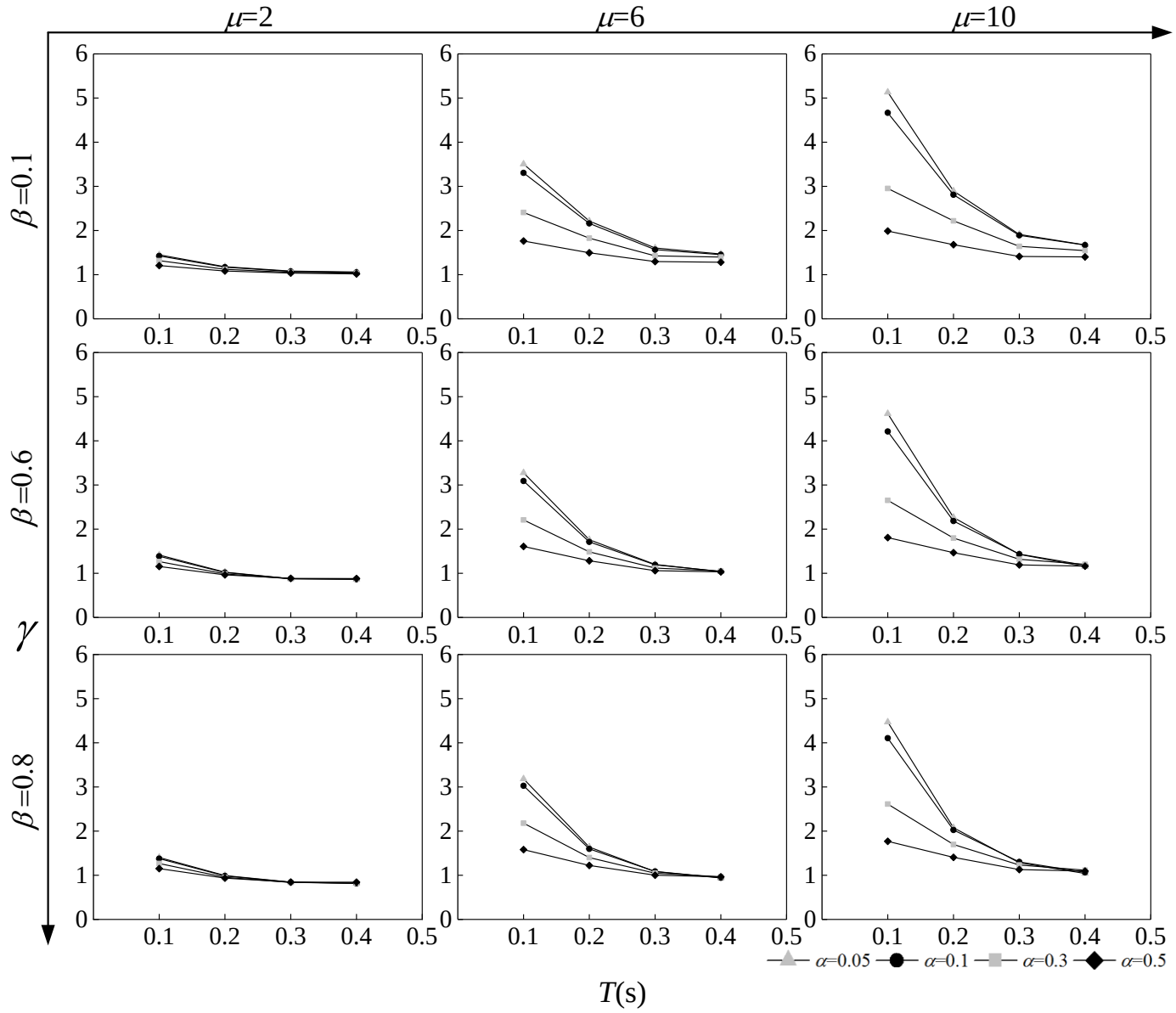

(a)

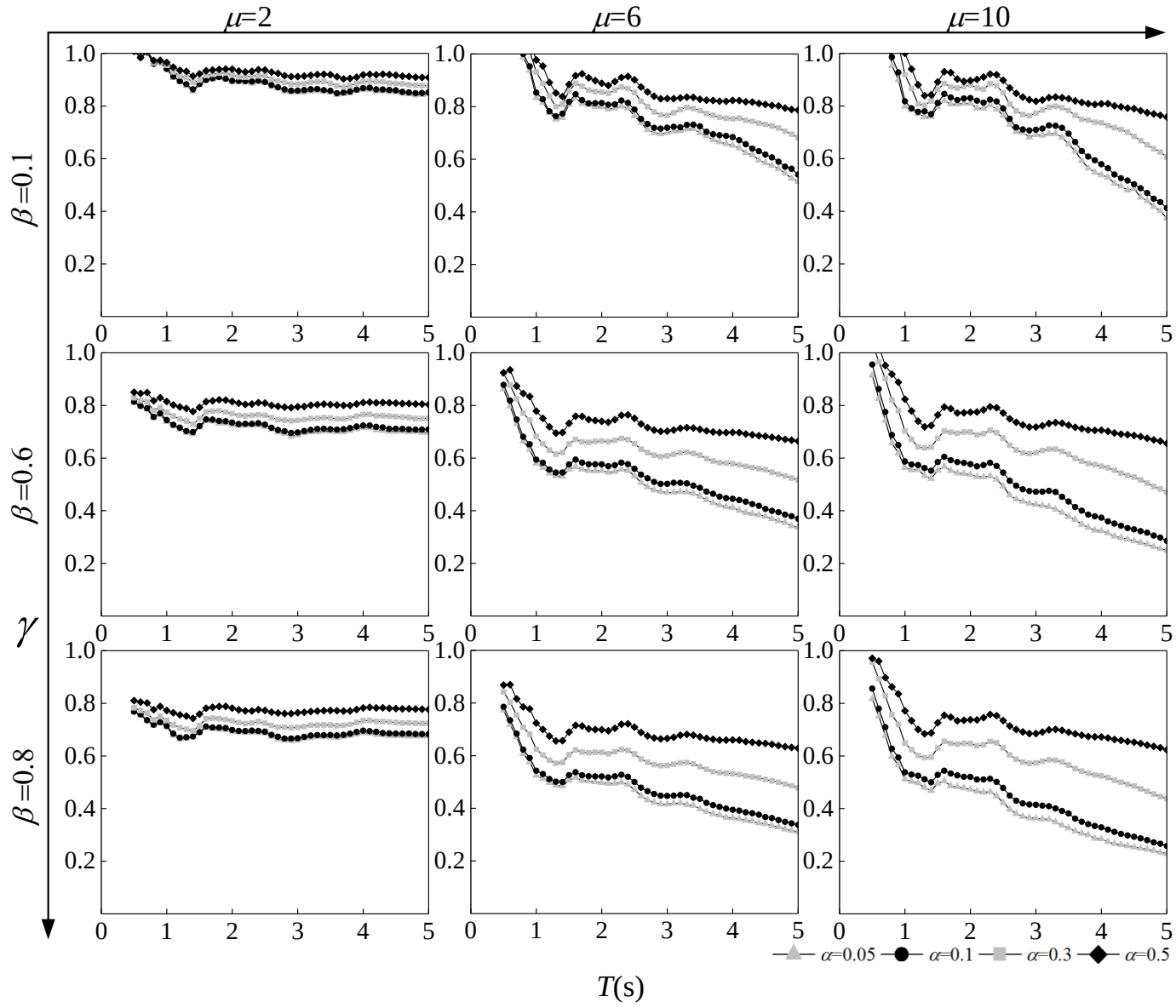

(b)

Fig. 5 Representative mean energy factor spectra.

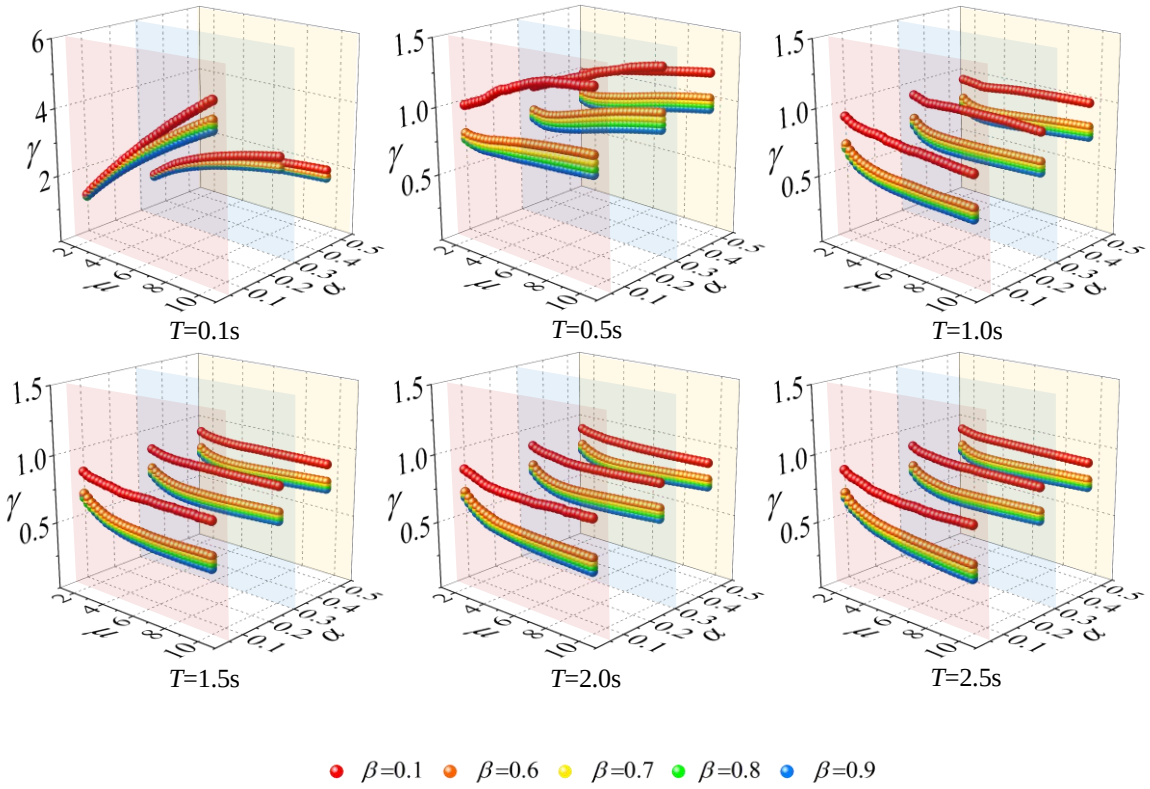

Fig. 6 Influence of hysteretic parameters on the mean energy factor.

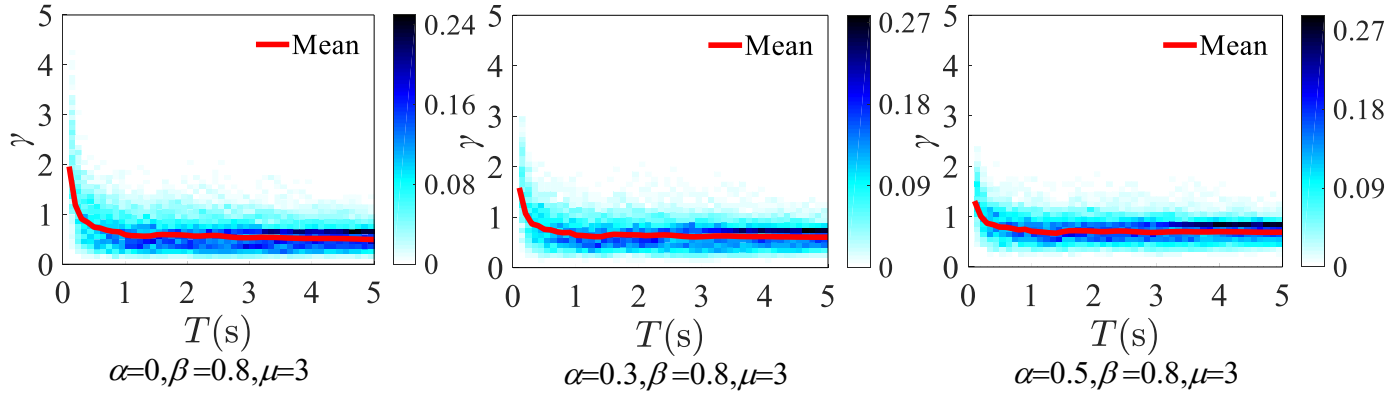

(a)

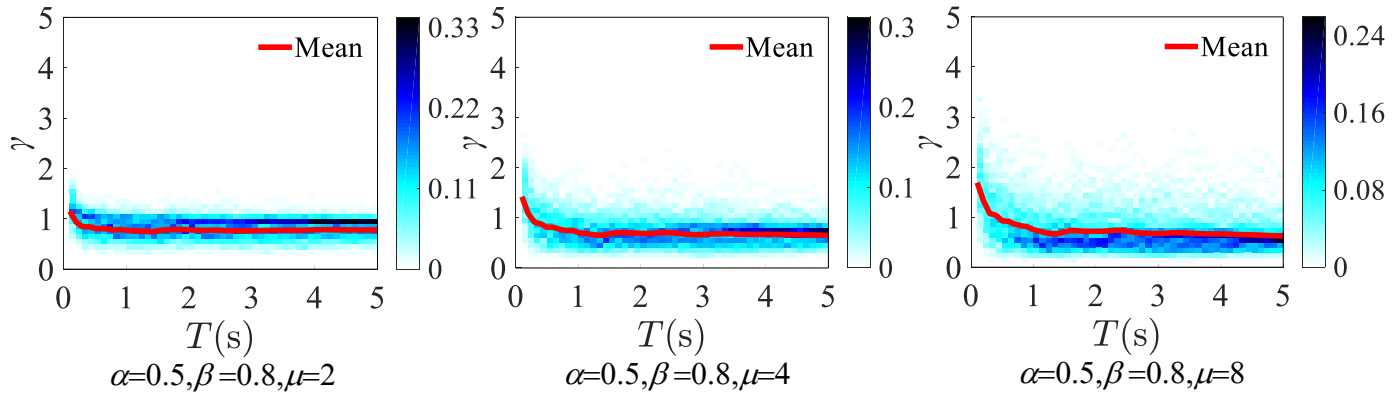

(b)

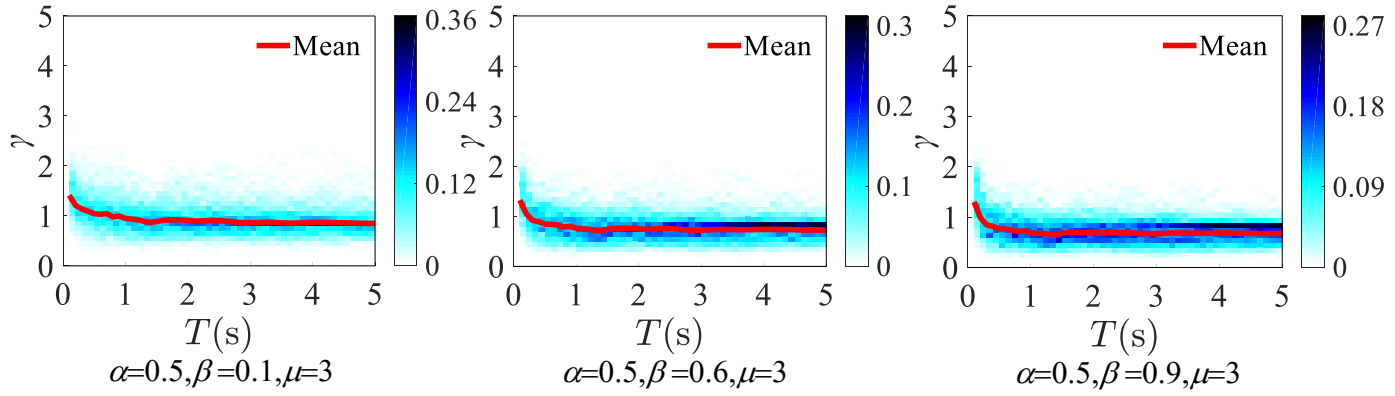

(c)

Fig. 7 Influence of hysteretic parameters on the dispersion of the energy factor.

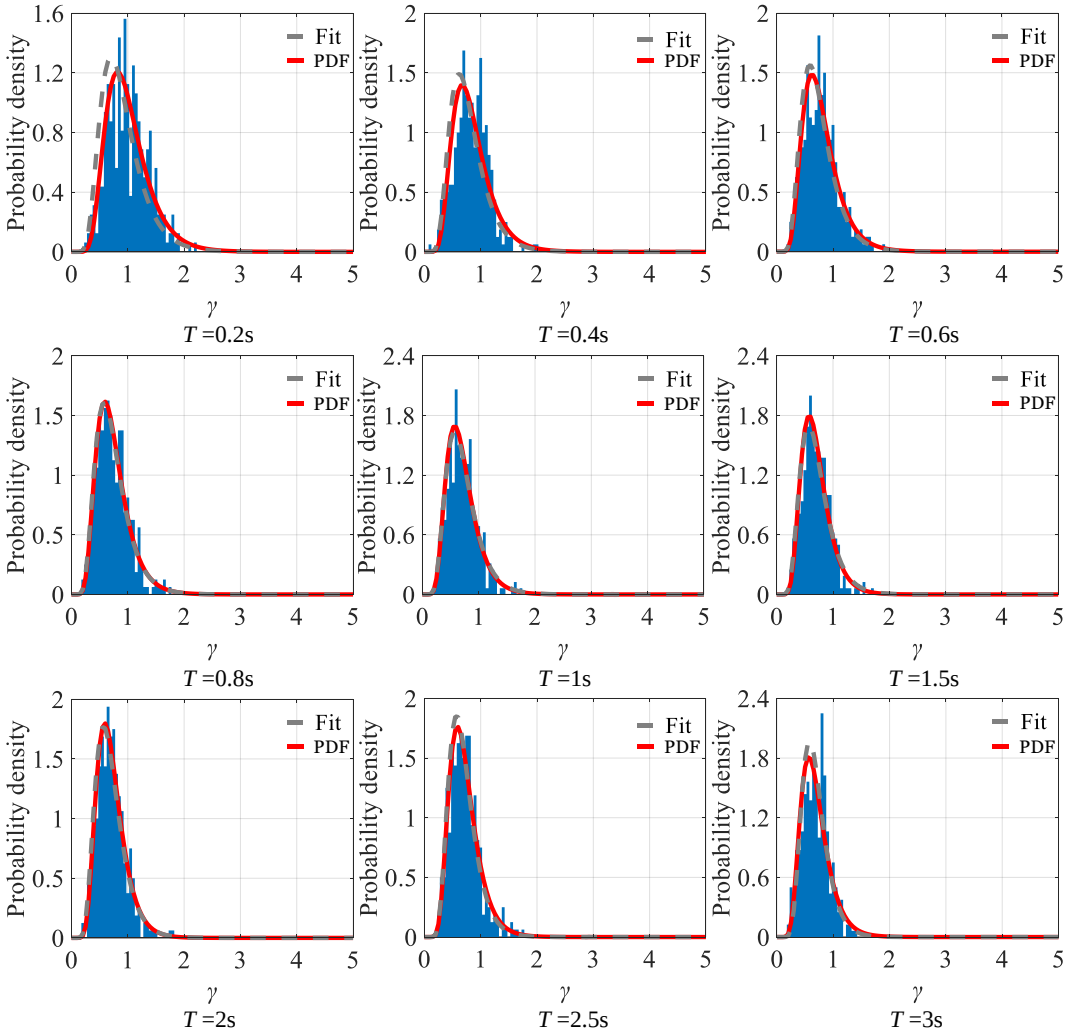

Fig. 8 Representative histograms and the corresponding probability density function curves of the energy factor.

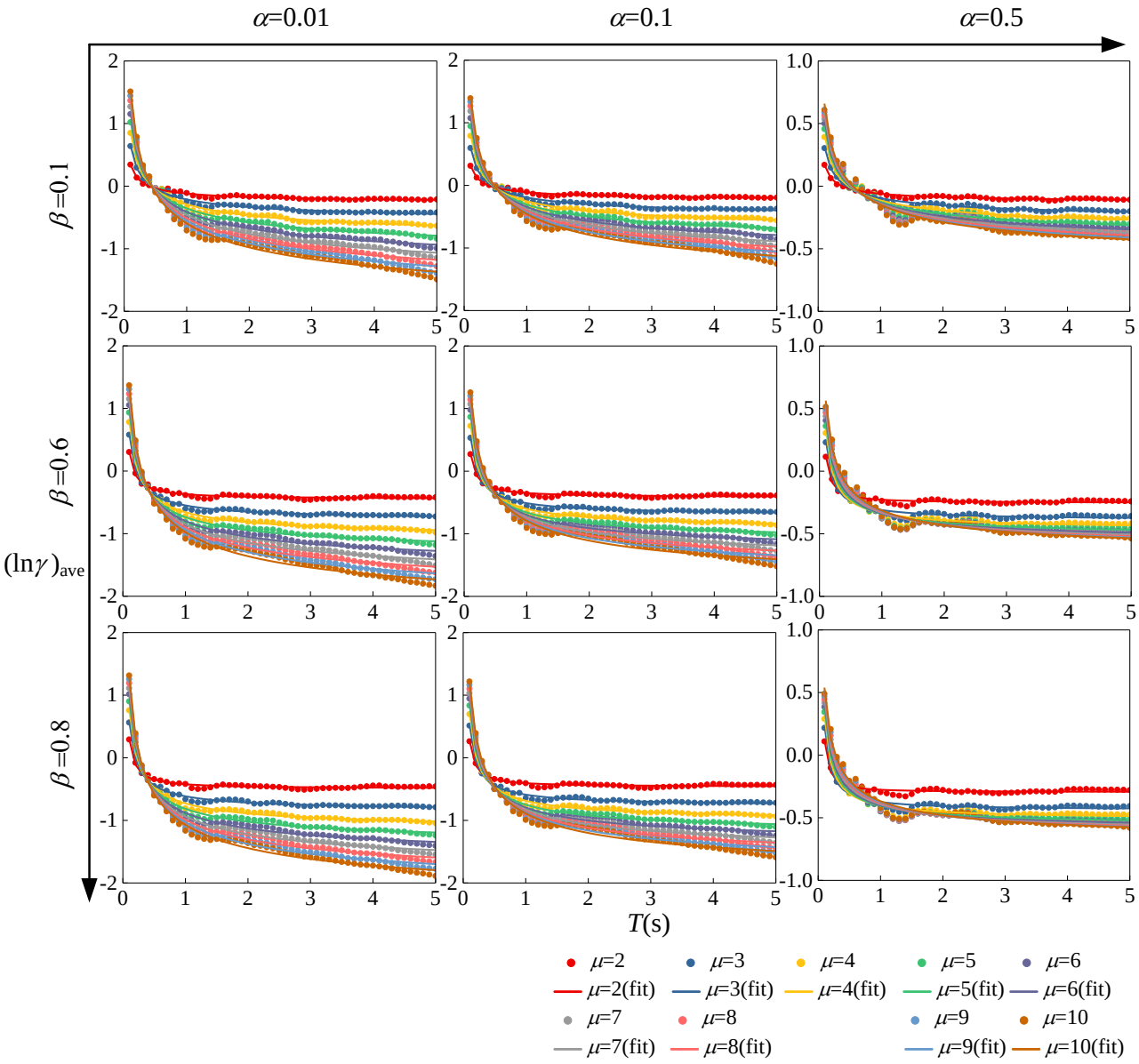

Fig. 9 Representative $(\ln \gamma)_{ave}$ - T spectra.

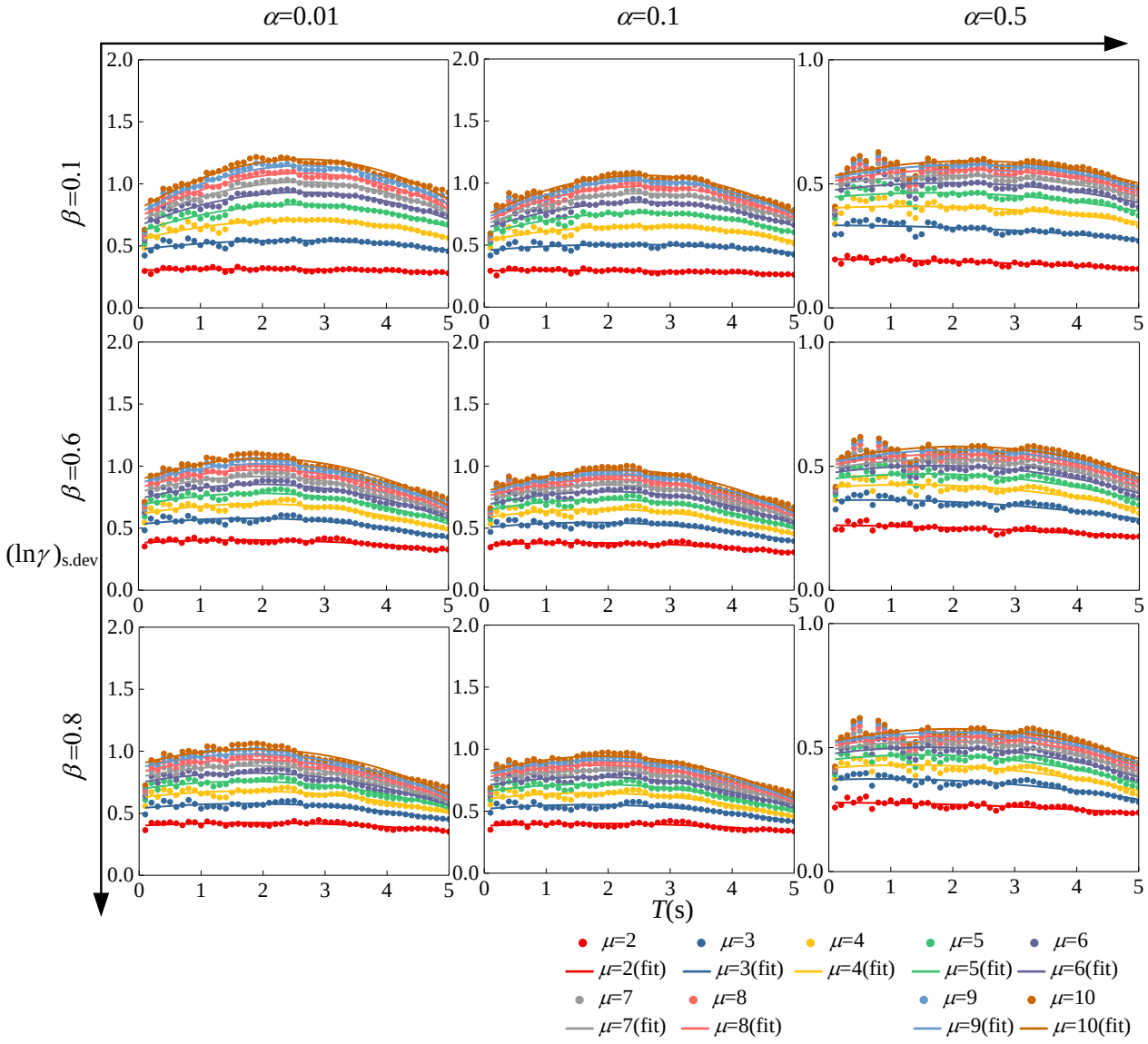

Fig. 10 Representative $(\ln \gamma)_{s,dev}$ - T spectra.

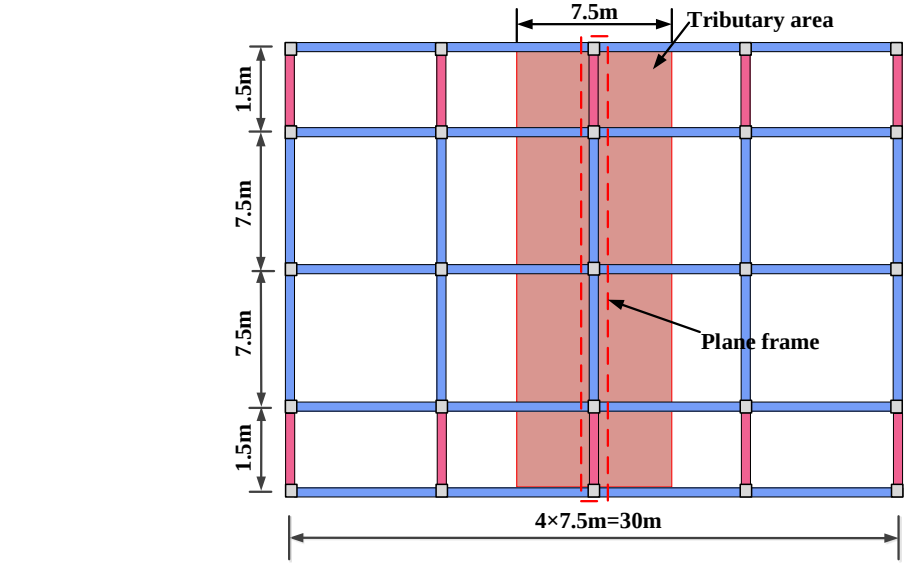

(a)

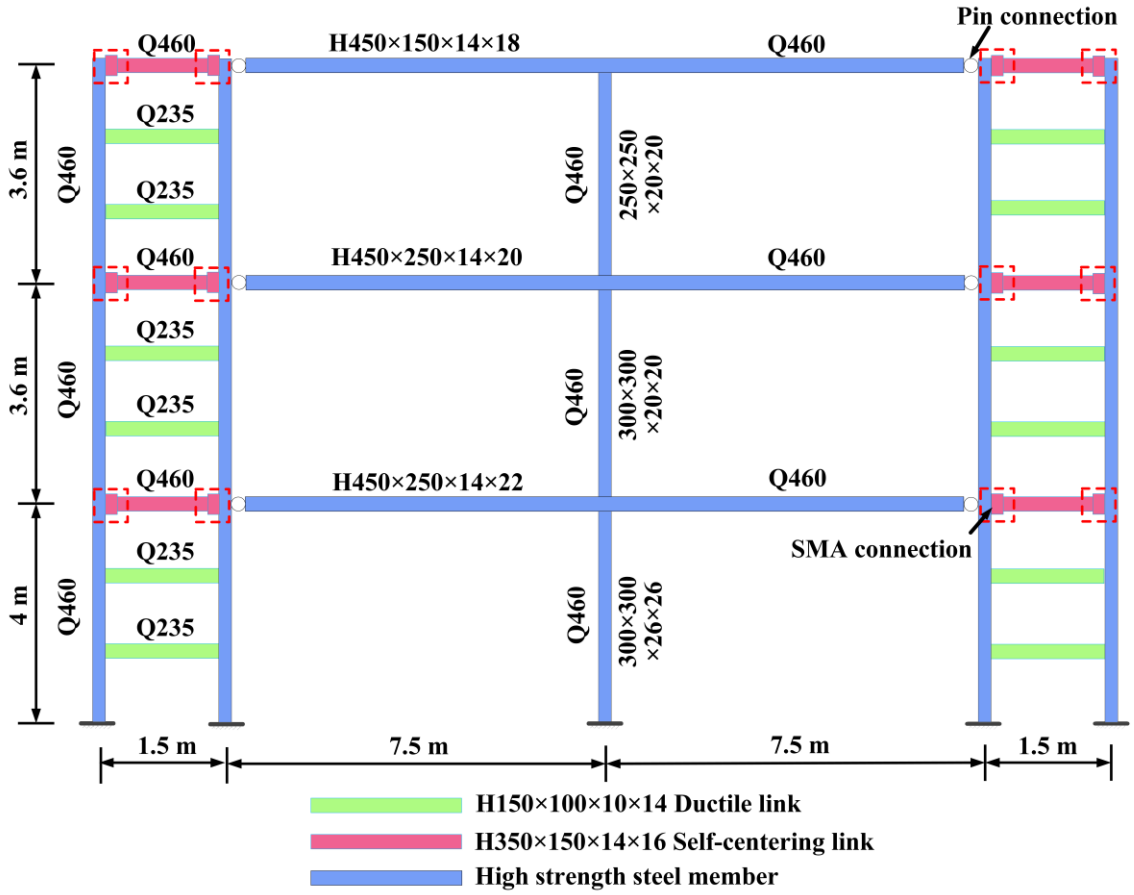

(b)

Fig. 11 Information on the prototype structure: (a) layout and (b) elevation.

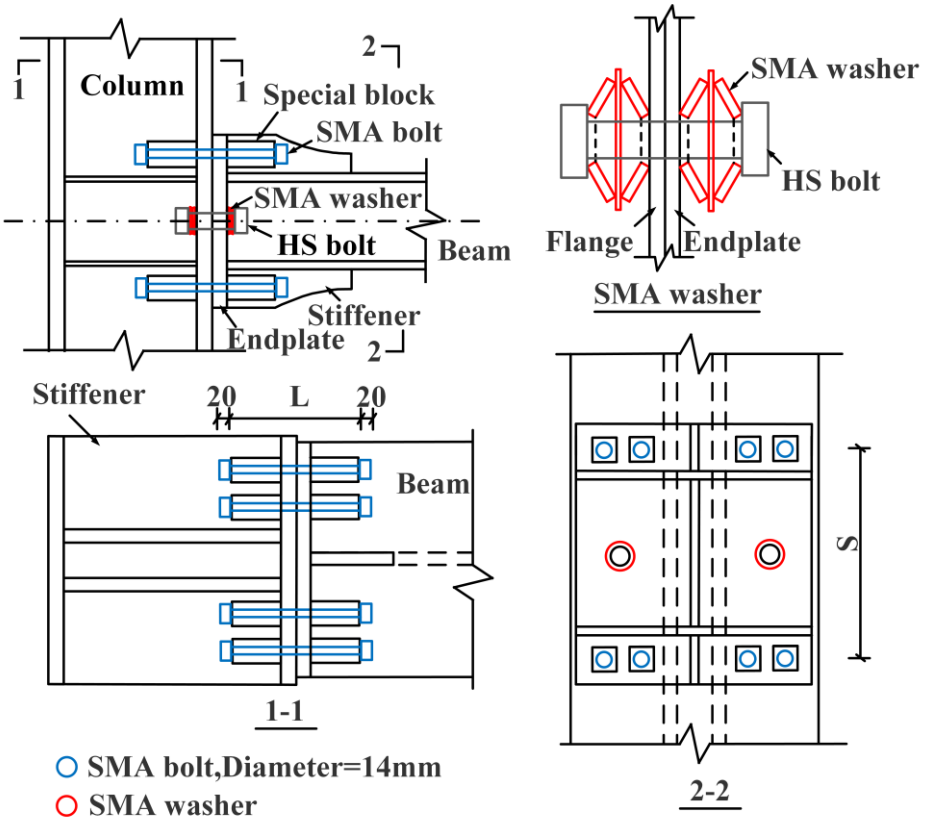

Fig. 12 Configuration of the SMA connections.

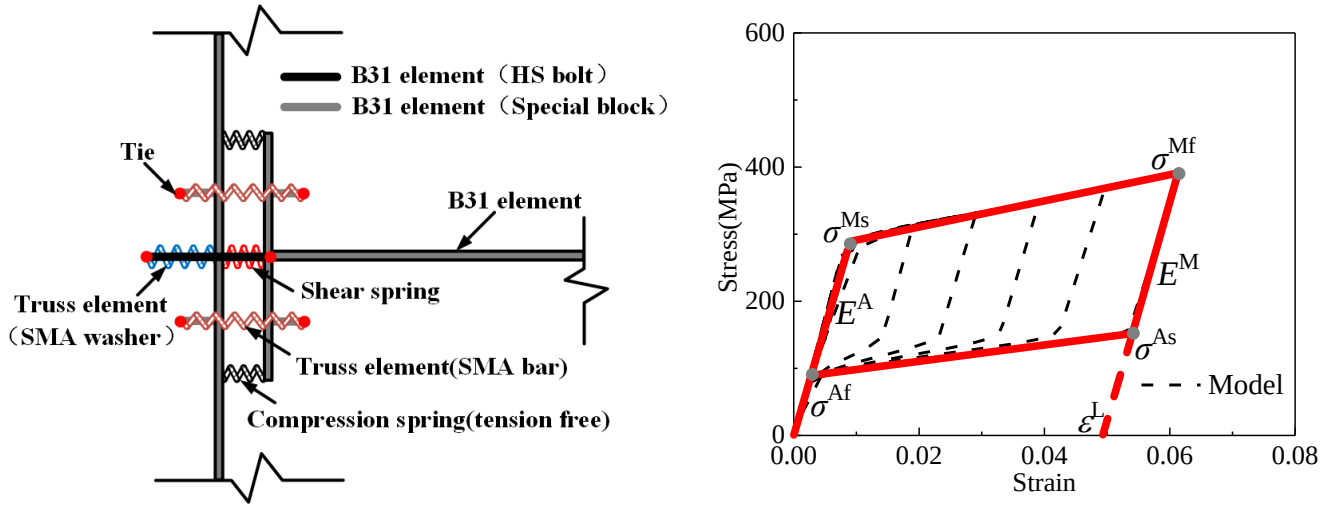

(a) (b)

Fig. 13 Simplified SMA connection model and material characteristics: (a) simplified model and (b) material model.

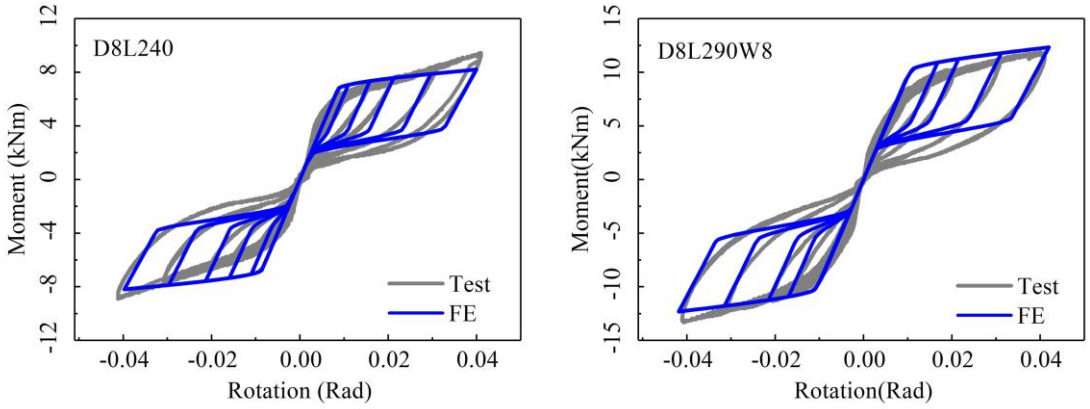

Fig. 14 Verification of the simplified connection model.

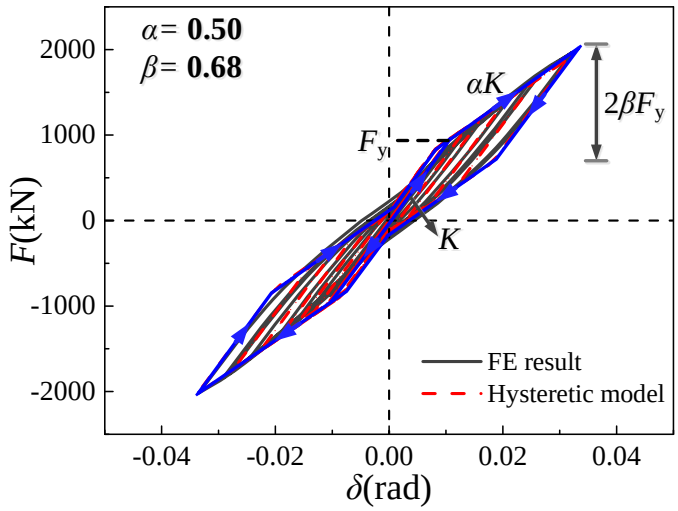

Fig. 15 Verification of the structural hysteretic model.

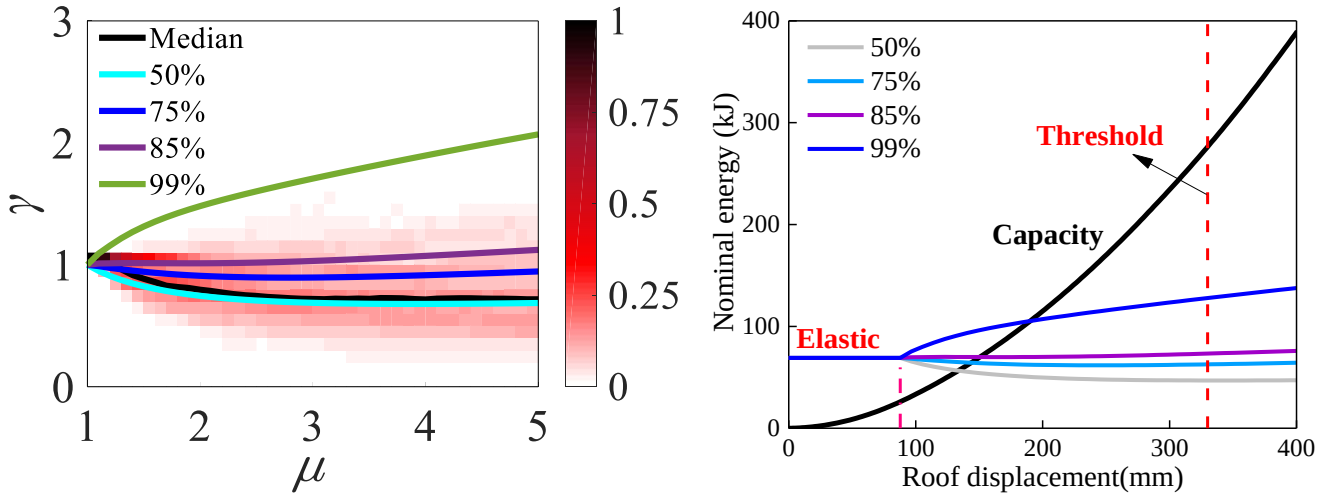

(a) (b)

Fig. 16 Probabilistic energy demand curves and capacity curves: (a) probabilistic energy factor spectra and (b) damage-control evaluation diagram.

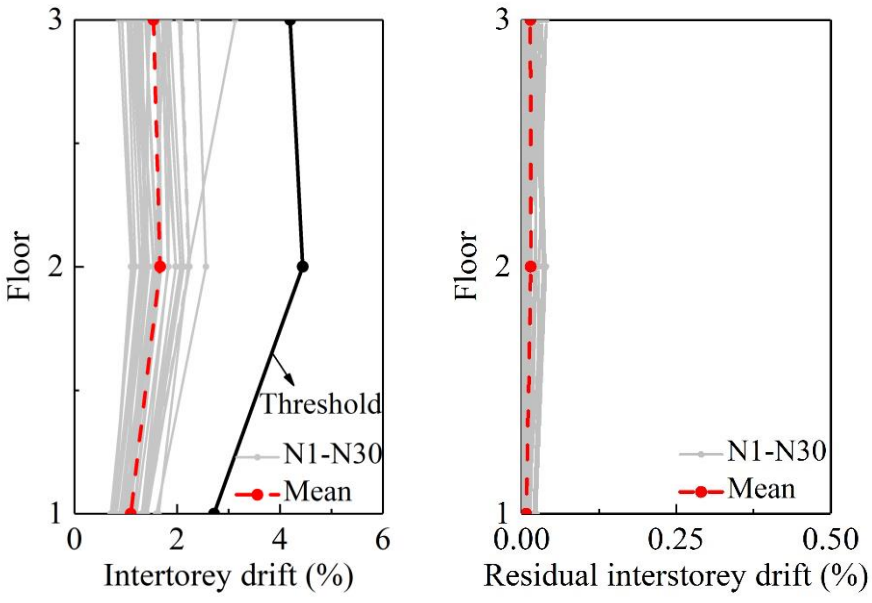

(a) (b)

Fig. 17 Analysis results by NL-RHA: (a) Peak interstorey drift and (b) residual interstorey drift.

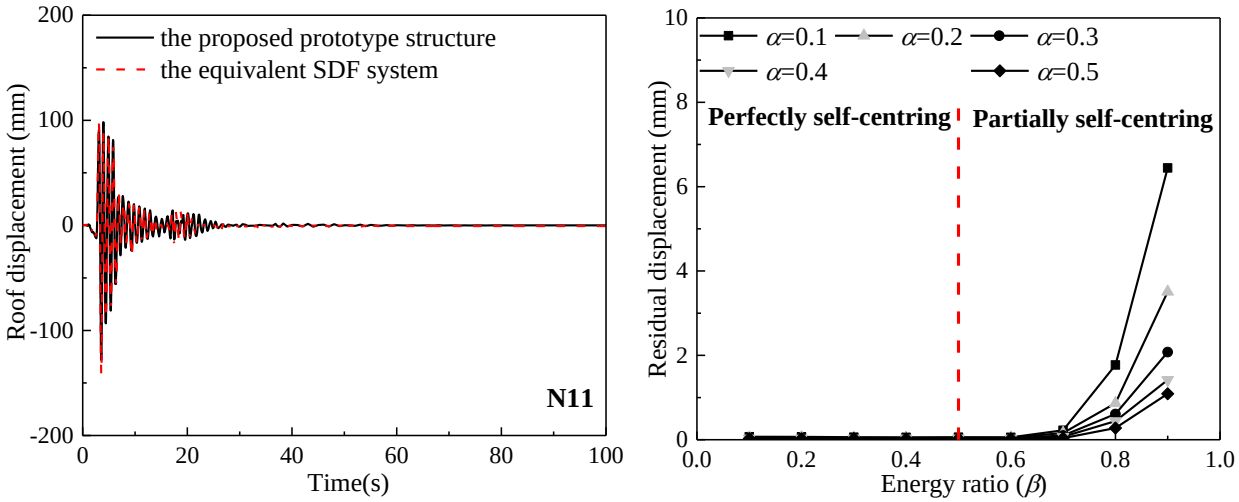

(a) (b)

Fig. 18 Seismic responses of the equivalent SDF system: (a) the roof displacement history responses and (b) the mean residual displacement responses.

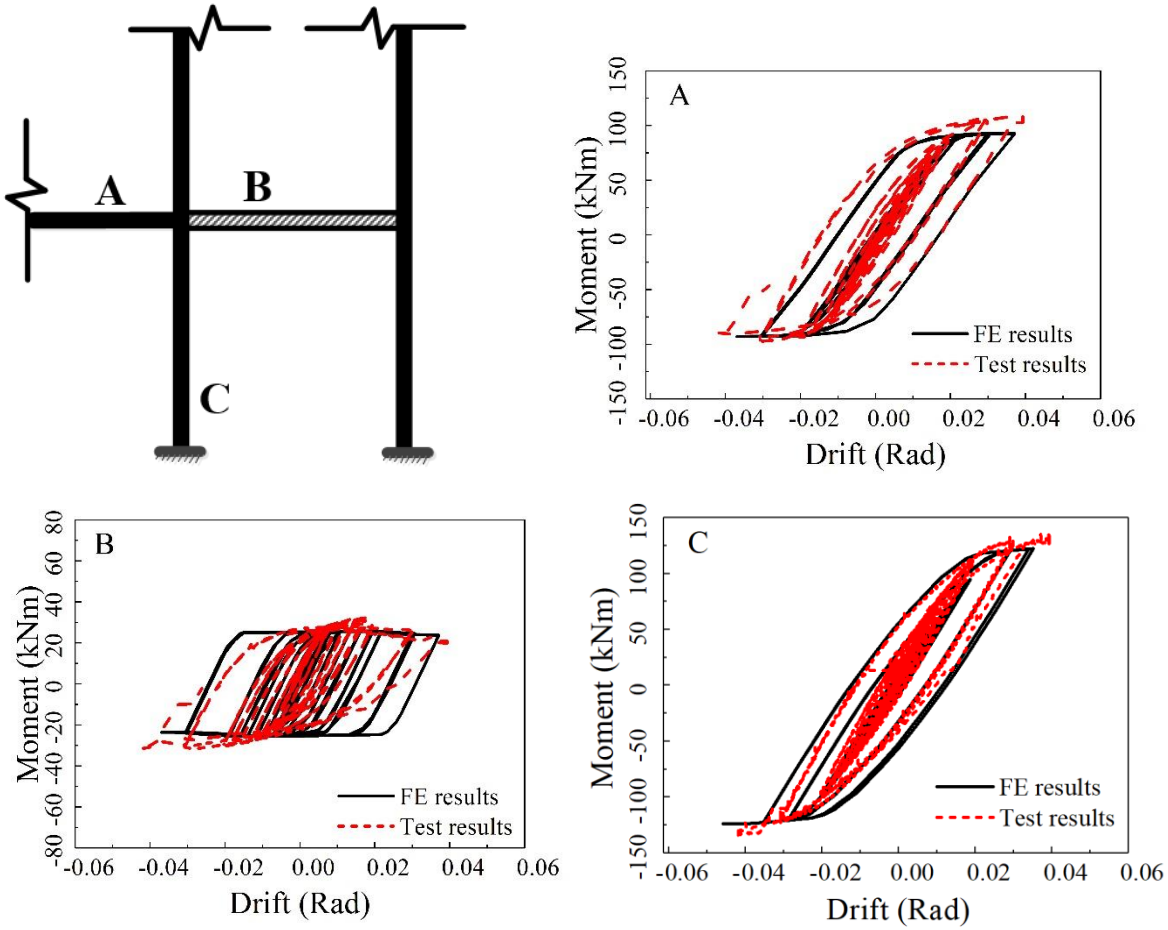

Fig. A1 Validation of the modelling techniques of main frame members and ductile links.

Table 1 SMA material properties used in the FE study [14]

Mechanical quantities	Values
Forward transformation start stress σ^{MS}	280 MPa
Forward transformation end stress σ^{Mf}	380 MPa
Reverse transformation start stress σ^{AS}	150 MPa
Reverse transformation end stress σ^{Af}	75 MPa
Austenite elasticity E^{A}	35 GPa
Martensite elasticity E^{M}	25 GPa
Maximum transformation strain ε^{L}	5%
Poisson's Ratio ν^{A}	0.33
Poisson's Ratio ν^{M}	0.33

Table 2 Dynamic properties of the prototype system

Property (unit)	*1st Mode*	*2nd. Mode*
Period (s)	0.83	0.26
Modal effective mass (t)	228.83	28.19
Modal participation factor	1.28	0.36

Table 3 Near-field earthquake motions for structural analysis

No.	Record	*M*	Distance (km)	PGA (cm/s^2)
N01	San Fernando, 1971, Pacoima Dam	6.61	1.81	1194.66
N02	San Fernando, 1971, Pacoima Dam	6.61	1.81	1213.55
N03	Coyote Lake, 1979, Gilroy Array #2	5.74	2.05	187.01
N04	Coyote Lake, 1979, Gilroy Array #2	5.74	2.05	250.44
N05	Coyote Lake, 1979, Gilroy Array #6	5.74	5.7	413.35
N06	Coyote Lake, 1979, Gilroy Array #6	5.74	5.7	312.46
N07	Irpinia_Italy-01, 1980, Bagnoli Irpinio	6.9	8.18	127.06
N08	Irpinia_Italy-01, 1980, Bagnoli Irpinio	6.9	8.18	185.95
N09	Irpinia_Italy-01, 1980, Sturno (STN)	6.9	10.84	222.13
N10	Irpinia_Italy-01, 1980, Sturno (STN)	6.9	10.84	314.11
N11	Mendocino, 1992, Petrolia	7.1	8.5	625.60
N12	C. Mendocino, 1992, Petrolia	7.1	8.5	642.24
N13	Erzincan, 1992	6.7	2	423.90
N14	Erzincan, 1992	6.7	2	448.29
N15	Landers, 1992	7.3	1.1	699.62
N16	Landers, 1992	7.3	1.1	783.89
N17	Nothridge, 1994, Olive View	6.7	6.4	718.16
N18	Nothridge, 1994, Olive View	6.7	6.4	583.79
N19	Kobe, 1995, Takatori	6.9	4.3	771.10
N20	Kobe, 1995, Takatori	6.9	4.3	416.11
N21	Elysian Park 1	6.9	17.5	842.50
N22	Elysian Park 1	6.9	17.5	875.07
N23	Elysian Park 2	7.1	10.7	1768.10
N24	Elysian Park 2	7.1	10.7	885.75
N25	Elysian Park 3	7.1	11.2	993.28
N26	Elysian Park 3	7.1	11.2	643.02
N27	Elysian Park 4	7.1	13.2	904.44
N28	Elysian Park 4	7.1	13.2	628.51
N29	Elysian Park 5	7.1	13.7	1139.20
N30	Elysian Park 5	7.1	13.7	499.29

Conflict of Interest

There is no financial/personal interest or belief that could affect our objectivity. There are no potential conflicts of interest either.

Author statement

Xuhong Zhou: Conceptualization, Writing-Reviewing and Editing, Supervision, Funding acquisition

Huanyang Zhang: Writing-Original draft preparation, Validation, Formal analysis , Methodology, Software

Ke Ke*: Conceptualization, Writing-Reviewing and Editing, Software, Methodology, Validation, Formal analysis, Funding acquisition

Lihua Guo: Visualization, Formal analysis, Software

Michael CH Yam: Resources, Writing-Reviewing and Editing, Project administration